A Numerical Study of Sediment Transport and Event Bed Genesis During Tropical Storm Delia

TIMOTHY R. KEEN[1] AND RUDY L. SLINGERLAND

Department of Geosciences, Pennsylvania State University, University Park

Some event beds (tempestites) are thought to be emplaced on shallow marine shelves by the combined action of strong coastal currents and high waves during fairly short-lived storms. To test this hypothesis, a storm sedimentation system has been constructed from six numerical models describing a cyclonic wind field, three-dimensional coastal circulation, wind waves generated over the continental shelf, the combined effect of steady and oscillatory currents within the benthic boundary layer, suspended and bed load transport of sediment, and conservation of the seafloor. This model system is used to hindcast winds, currents, waves, and resulting sedimentation during Tropical Storm Delia, which passed over the Texas-Louisiana shelf on September 3-4, 1973. Sensitivity to the initial substrate is investigated in four experiments using uniform silt, uniform sand, a mud line at the 20-m isobath, and a simplified modern sediment distribution. Modeled coastal currents are vertically uniform and do not reveal the structure predicted by the mid-latitude geostrophic storm circulation model, because the predicted depth of the wind-mixed layer is greater than the water depth over the shelf. Shelf currents in excess of 2 m/s flow predominantly along the coast to the southwest during most of the storm, driven by the wind stress and the trapped coastal wave which peaks at 180 cm near Galveston. Significant wave heights reach 8 m on the outer shelf but are less than 4 m over the inner shelf. These waves combine with steady currents to produce bed shear velocities which locally exceed 20 cm/s. The region of highest stresses always lies to the right of the storm track (viewed down the path) and moves across the shelf with the eye of the storm. Three general sediment transport paths are evident: (1) onshore transport of finer sediment over the outer shelf to the right of the storm track, (2) westward-directed along-shelf transport of predominantly fine sediment between approximately 40-m and 20-m water depths, and (3) minor offshore transport of sand from the shoreface to depths less than 30 m. The resulting event bed has a ragged appearance with a maximum thickness of about 20 cm in region 1, and covers an area of approximately 3×10^4 km^2 to the right of the storm track. Aside from local transport associated with finer sediments, these results are relatively insensitive to initial sediment type. Comparison of model results to observed data from Buccaneer platform shows that the different models performed adequately during the peak of the storm, except for a significant underprediction of the significant wave height by the wind sea model. The estimated uncertainty in the calculated combined shear stresses u_*, based on errors produced by the individual model components, is most dependent on the wave bottom orbital amplitude. The total uncertainty in u_* is estimated to be approximately 7%.

1. INTRODUCTION

Ancient shallow marine clastic deposits often consist of thick shale sequences punctuated by discrete, laterally continuous sandstone beds. The sandstone beds commonly possess sharp, erosive bases and an internal facies organization wherein coarse, structureless basal sandstones evolve upward into hummocky-stratified, very fine grained sandstones. Bed tops are often silty, wave rippled, and burrowed [e.g., *Goldring and Bridges*, 1973; *Bouma et al.*, 1982; *Einsele and Seilacher*, 1982; *Harms et al.*, 1982; *Atkinson et al.*, 1986; *Brenchley et al.*, 1986; *Swift et al.*, 1987; *Craft and Bridge*, 1987]. To understand the origin of these beds, researchers have turned to studies of storm-induced bottom flow and sediment transport on modern shelves [*Hayes*, 1967; *Kumar and Sanders*, 1976; *Sheng*, 1983; *Denness*, 1984; *Swift et al.*, 1986; *Vincent*, 1986; *Kachel and Smith*, 1986; *Nittrouer et al.*, 1988; *Morton*, 1988]. Especially important was *Hayes'* [1967] work on some Texas continental shelf deposits after the passage of Hurricane Carla in 1961. Hayes proposed that sheet sands were emplaced offshore during the waning of the hurricane's strength, as the storm surge ebbed and flow was directed offshore under

gravity. This conclusion was based on the offshore thinning and fining pattern observed within the Hurricane Carla bed. This concept was subsequently challenged by workers who proposed that geostrophic currents were the agent of sediment transport [*Morton*, 1981; *Niedoroda et al.*, 1984; *Swift and Niedoroda*, 1985; *Nummedal and Snedden*, 1987; *Snedden et al.*, 1988]. At the same time, other workers [e.g., *Walker*, 1984], attempting to reconcile offshore-directed sole marks, proposed that dilute turbidity currents were responsible. Presently, there is a growing consensus that deposits of this sort were emplaced by combined steady and oscillatory flow fields under fairly short lived storms [*Dott and Bourgeois*, 1982; *Brenchley*, 1985; *Duke*, 1985; *Nummedal and Snedden*, 1987; *Duke*, 1990; *Duke et al.*, 1991], possibly justifying the appellation "event bed" or "tempestite."

Definitive proof of a storm origin is still hard to come by, however. No one has ever witnessed the emplacement of a storm deposit or the bed dynamics that produce such alleged storm indicators as hummocky cross-stratification. Indeed, the very nature of storm deposits (their regional extent and the violent processes that form them) makes field and flume observations of the relationship between sedimentation and resulting strata difficult. While probably physically viable, sediment transport by combined storm-generated geostrophic flows and oscillatory water waves remains a conjecture for the origin of these beds.

This state of affairs convinces us that a numerical model of event bed genesis could provide a test of the storm model, as well as provide useful predictions to help guide future observations. Toward this end we have combined six numerical models into a Storm

[1] Now at Institute of Marine and Coastal Sciences, Rutgers University, New Brunswick, New Jersey.

Sedimentation System (S^3) to predict erosion, transport, and deposition at the shelf-wide scale as functions of the wind field of a tropical cyclone. The six models are (1) a wind forecasting model, (2) a three-dimensional coastal ocean circulation model, (3) a wind sea prediction model, (4) a combined current-wave benthic boundary layer model, (5) a suspended and bed load sediment transport model, and (6) a bed conservation model. The emphasis in the system is placed on processes operating in water depths greater than 10 m. Although the shoreface is recognized as being the most important source of sediment to the storm sediment pool, as well as the location of the thickest storm beds in ancient sequences, it is not modeled in this study, because the scale of processes there is smaller than that of a numerical grid compatible with the shelf scale.

This paper first describes S^3 and its operation. Then the numerical results for coastal circulation, the wind sea, and the combined seafloor shear stresses during Tropical Storm Delia are described. Several numerical experiments follow which test the sensitivity of computed sediment transport and event bed characteristics to various initial bed textures. Finally, we discuss uncertainties in model output, the structure of coastal storm currents, and the expected regional extent and characteristics of a single storm deposit produced by a storm of specific magnitude and track.

2. THE STORM SEDIMENTATION SYSTEM

The components of S^3 are not coupled in this study, because the intent was to evaluate each model separately and determine if it was possible to use the output from wave and circulation models to calculate combined current-wave sediment transport during a severe storm. Furthermore, problems encountered within individual model components necessitated compromises which decreased their performance. Part of the problem lay in limitations on computer resources, part in the time to be allotted to the work, and part in the failure of system components to operate properly under the range of conditions encountered during a tropical cyclone.

2.1. Winds, Currents, Waves, and Combined Shear Stresses

The circulation and wave models require winds at a height of 20 m. These were supplied by the empirical model of *Harris* [1958], with a correction for a moving storm after *Jelesnianski* [1966]. The wind field is cyclonic, with vectors orthogonal to radii through the storm eye and turned inward by a deflection angle of 20°. The grid position and bearing of the storm center are input periodically, with the location of the eye interpolated between grid points. This wind field applies only to the area directly influenced by the maximum storm winds, since it cannot capture synoptic-scale patterns related to the cyclone. Its accuracy was evaluated using data collected by *Forristall et al.* [1977] at the Buccaneer oil production platform, situated 45 km offshore of Galveston, Texas. Both predicted wind speed and direction (Figure 1) compare favorably with those observed.

Coastal ocean circulation for S^3 is calculated by the three-dimensional turbulent-energy closure model of *Leendertse et al.* [1973], which solves the primitive equations of turbulent flow in a Cartesian coordinate system using an explicit finite-difference method, with an implicit solution found for the vertical exchange of momentum, heat, turbulence, and mass. Details of the mathematical formulation used in this study are given in Appendix A. It has been evaluated for San Francisco Bay, Chesapeake Bay [*Leendertse and Liu*, 1977], the Bering Sea [*Liu and Leendertse*, 1978], Long Island Sound [*Leendertse and Liu*, 1978], and Bristol Bay [*Liu and Leendertse*, 1979]. Such detailed testing has not been

accomplished for severe storms, but several numerical experiments were completed in the course of this work to evaluate model results with respect to theoretical predictions and published numerical results. The circulation patterns computed for several hurricanes within the western Gulf of Mexico revealed features commonly associated with tropical cyclones: vertical and horizontal inertial oscillations in deep water, horizontal shear at the shelf break, an enhanced convergence zone with path changes, and barotropic shelf waves [*Keen*, 1992]. Further, the numerical results for Hurricane Gilbert [*Keen and Slingerland*, 1993] can be qualitatively compared to those for Hurricane Allen [*Cooper and Thompson*, 1989] because of the similar paths taken by the two storms. The flow fields computed by the two models were similar, with peak velocities of about 150 cm/s on the shelf near Galveston and southward flow of almost 50 cm/s along the Mexican coast. The inertial oscillations produced within the wake were of the order of 100 cm/s for both models. Furthermore, the mixed-layer depths calculated by S^3 were also similar in magnitude and distribution to those computed by Cooper and Thompson. Although this is not considered a rigorous test of the turbulent flow model's performance during severe storms, it suggests that the calculated flow field is reasonable. A quantitative comparison of model-calculated flow and observations during Tropical Storm Delia will be made in sections 4.1 and 5.1.
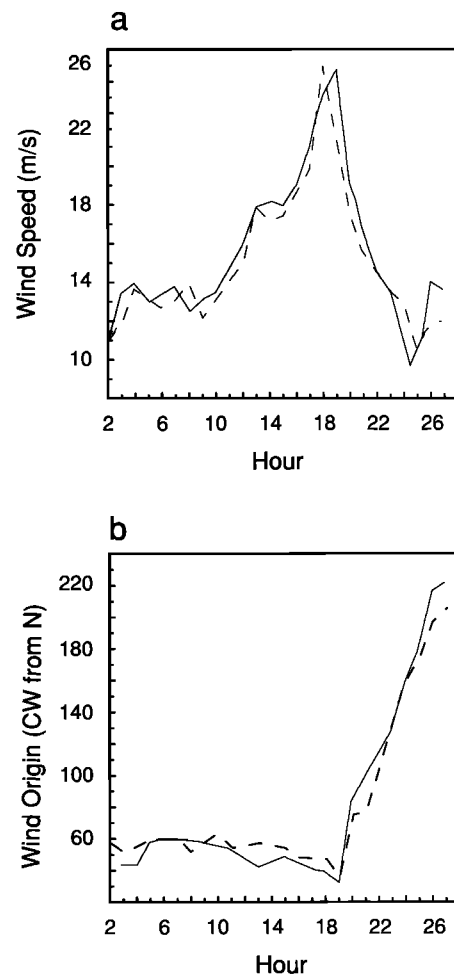

Fig. 1. Modeled versus observed wind field at Buccaneer platform. The dashed line represents the output from the cyclone wind model, and the solid line is the averaged observed values reported by *Forristall et al.* [1977]. (a) Wind speed, in meters per second. (b) Wind source, in degrees clockwise from north.

The wind sea is computed using a simplified version of the finite-depth wave model of *Graber and Madsen* [1988] (hereinafter referred to as GM) which neglects swell. A comparison of results from the simplified version with those of GM for the full model is presented in Appendix B, along with comparisons of observed and computed spectra for two historical storms. The results initially suggested that the reduced model is adequate for the area directly affected by storm winds. In order to calculate bottom wave orbital parameters, the significant wave height $H_{1/3}$ and peak wave frequency f_m must be known. $H_{1/3}$ equals $4\sqrt{E_T}$, where E_T is the total energy of the wave spectrum, and f_m is calculated by the wind sea model. From the known values of $H_{1/3}$ and f_m the wave parameters required for the boundary layer calculations are found from linear wave theory. The maximum orbital excursion amplitude A_b is given by $a/\sinh kh$, and the maximum orbital velocity U_b is given by $A_b\omega$, where a is the surface wave amplitude, k is the wave number, h is water depth, and ω is the radian frequency.

Because of the importance of waves during storms, the wave-dominated benthic boundary layer theory of *Glenn and Grant* [1987] is used to calculate the effective shear stress at the seafloor in the presence of steady and oscillatory currents. The original FORTRAN program (NBM87) is used, with only those changes required to integrate it as a subroutine into our sediment transport program. It requires as input (1) the current speed and direction relative to the waves at a reference height z_r, (2) the peak wave bottom velocity and excursion amplitude, and (3) the diameter, relative density, concentration in the bed, particle fall velocity, and critical Shields parameter for all available size classes.

2.2. Sediment Transport and Bed Conservation

Sediment transport and bed continuity follow the works by *van Niekerk et al.* [1992] and *Vogel et al.* [1992], with expansion to two horizontal dimensions. The bed load transport rate of sediment size class n is given by

$$i_{bn} = P_n \frac{A'}{\tan\alpha}(u_* - u_{*_n})(\tau_o - \tau_n) \quad (1)$$

where P_n is the volumetric concentration in the bed; A' is a parameter equal to $\log(z_b/k_b)/\kappa$, with κ, von Karman's constant, z_b, the distance above the bed to the center of thrust on bed load grains, and k_b the physical bottom roughness; $\tan\alpha$ is a dynamic friction coefficient; u_* is the combined current-wave shear velocity; u_{*_n} is the critical shear velocity for sediment class n; τ_o is the combined shear stress; and τ_n is the critical shear stress for class n. The term $A'/\tan\alpha$ is set constant to 10 as in the work by *van Niekerk et al.* [1992]. The direction of bed load transport is collinear with the mean wind sea direction θ_o; if it is within $\pm90°$ of the steady current direction, the bed load transport vector is identical to θ_o, whereas if the angle exceeds $90°$, the bed load travels opposite to θ_o. Although not too accurate, this approximation does allow waves to exert a primitive control on bed load transport. As it turns out, the direction chosen for bed load transport is insignificant in this study because suspended load dominates.

Suspended sediment is transported by the steady currents calculated for the lowermost circulation model level. The suspended sediment concentration profile for each size class is predicted by

$$c_{mn} = c_{bn}\left[\frac{h-z}{z} \times \frac{a_o}{h-a_o}\right]^{\left(\frac{w_{fn}}{\kappa u_{*c}}\right)} \quad (2)$$

where c_{bn} is the concentration of class n at height a_o (the height of the moving bed layer), z is the height above the bed, and w_{fn} is the fall velocity. The reference concentration c_{bn} is calculated within the moving bed layer by $i_{bn}/(u_{bn}a_og)$, where u_{bn} is the near-bed velocity of size fraction n and g is the gravity constant. The total suspended load transport rate for a given size class is found for the x axis from

$$S_{sn} = \Delta_y \int_{a_o}^{z_r} u_r c_{mn} dz \quad (3)$$

where Δ_y is the grid dimension along the y axis.

To allow for evolving bed textures, an active layer is defined to be that part of the bed which interacts with the flow during one time step [*Rahuel et al.*, 1989]. Exchange occurs for each size fraction between the active layer and the overlying moving bed layer during each time step; erosion removes material from the subjacent bed, whereas deposition raises the active layer by an amount equal to the thickness of deposited sediment. The bed concentration P_n thus evolves with time to reflect the changing seafloor texture.

To account for mass exchange between the bed and the flow, the x direction bed conservation equation is written as

$$\rho_s(1-v)\frac{\partial}{\partial t}(\Delta_y z_n) + \frac{1}{g}\frac{\partial}{\partial x}(\Delta_y i_{bn}) + \frac{\partial S_n}{\partial x} = 0 \quad (4)$$

where ρ_s is the sediment density, v is the bed porosity, and z_n is the bed elevation due to size class n. The y direction conservation equation is of similar form. Solution of both equations is by a centered difference scheme that uses grid points both upflow and downflow from the current grid point.

2.3. Model System Operation

S^3 consists of the above models run serially, without coupling. The circulation model grid is used as a primary grid for model output. The wind stress is applied directly to this grid, whereas the wind sea requires a $45°$ rotation of wind stresses. Combined current-wave shear stresses are then found using computed wave parameters and steady currents calculated by the circulation model for the lowest model level present at each grid point. These currents are assigned a height of 10 m above the bottom; this reference level is slightly high for the linear eddy viscosity model but should be accurate within 5%, and the turning angle predicted by the boundary layer model is less than $10°$ for this height [*Grant and Glenn*, 1983].

Because the models are not presently interactive, they must be run in a specific sequence as seen in Figure 2. For this study, output from the wind model was saved every simulation hour for use in the circulation and wave models. No spin-up was used for the circulation model, and the initial condition was static. The wind sea was allowed to develop for 10 simulation hours before the calculations proceeded, with hourly output coinciding with circulation model results. The bed shear stresses, sediment transport, and bed continuity are calculated in a separate program at time steps of 1 hour.

The original intent was to use the suspended sediment transport from the boundary layer model to calculate sedimentation, but it was found to be unstable for the range of wave-current conditions encountered during the simulation. In order to maintain consistency, equation (2) was used to calculate the sediment profiles for
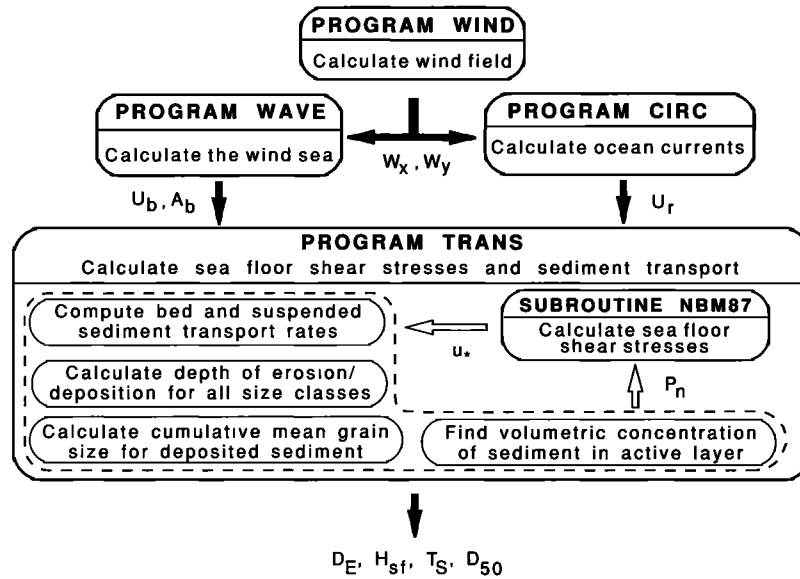
Fig. 2. Schematic flow chart for operation of the Storm Sedimentation System. See text for explanation.

all grid points. The parabolic eddy viscosity assumption implicit in (2) is undesirable but probably acceptable for this simple approach because of the lack of density stratification in the homogeneous water column and the neglect of feedback between physical processes represented by the individual models. This much simpler formulation produced lower transport rates than predicted for the boundary layer model (Figure 3), however, dispelling the concern that erosion would be overpredicted because of this simplification. Nevertheless, the concentration profiles used in damping turbulence within the boundary layer model are dependent on the changing reference concentrations P_n, which are also used for finding bed load transport rates i_{b_n} for use in (2). After the sediment transport rates are computed from (1) and (3), seafloor elevation changes for the current time step are calculated from (4). The following storm bed variables are produced at specified intervals during the simulation: the depth of erosion into the initial seafloor D_E; the seafloor elevation H_{sf}; the thickness of the bed produced by the storm, T_S; and the volumetric median grain size for the bed, D_{50}.

3. EXPERIMENTAL DESIGN FOR TROPICAL STORM DELIA

The numerical experiments described in this paper were designed to hindcast the sedimentary processes and regional sedimentation patterns produced by Tropical Storm Delia, which crossed the Texas shelf in September 1973 (Figure 4), using data reported by Forristall et al. [1977]. The region of interest is represented by a 33 × 67 model grid using a horizontal grid spacing of 13.5 km. This grid is rotated 57° clockwise to optimize the fit along the Texas coast. The water column is represented by nine levels with uniform thicknesses throughout the grid. The upper four levels are each 10 m thick; the fifth through the seventh are 20 m thick; the next-to-bottom level is 100 m thick; and the lowermost is 300 m thick. The passage of Delia across the northwest Gulf of Mexico, from 1700 CDT September 3 to 2100 September 4, was simulated using 1680 time steps of 60 s each for circulation and wave calculations and 28 time steps of 1 hour each for combined benthic boundary layer and sediment transport computations. References to hours in the following discussion refer to simulation hours, with hour 0 equivalent to 1700, September 3.

Horizontal boundaries for calculation of the flow field allowed

no flow. The landward boundary condition for bed conservation was chosen to simulate erosion of the sandy shoreface. Sediment for all size classes greater than 4 φ (0.064 mm) was introduced at a rate equivalent to the rate of erosion from any grid point adjacent to land. The lower boundary for the circulation model was formulated as described in Appendix A, with values of Chezy's C ranging from 500 to 1000 $cm^{1/2}/s$. Although these values may seem high, they are believed to adequately describe the range of seafloor and oceanographic conditions expected for the region. This is considered especially important because of overdamping of coastal flows when combined wave-current friction factors are used without sediment stratification corrections (S. M. Glenn, personal communication, 1992). The wave friction factor f_w was constant at 0.015. Within the benthic boundary layer model, the roughness height k_b was set to 2 cm and the sediment roughness to 0.09 mm. Values used for bottom friction coefficients in the circulation,
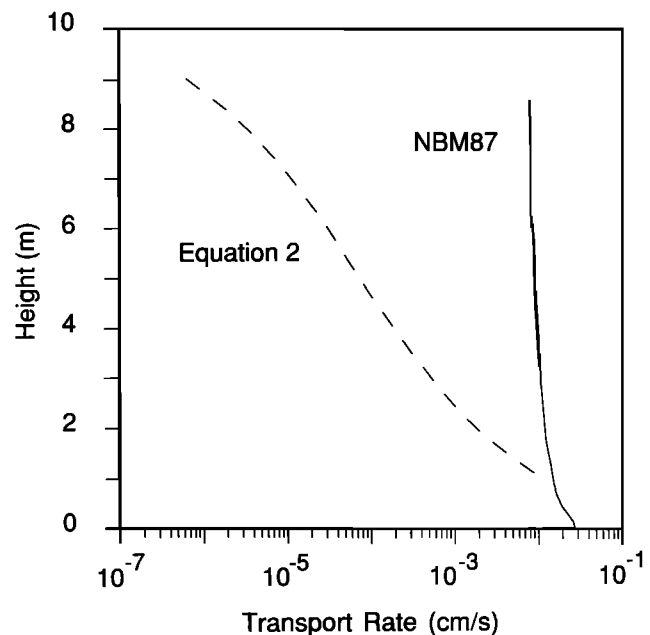

Fig. 3. Comparison of suspended sediment transport rate profiles for hour 18 at Buccaneer using equation (2) and the original NBM87 formulation.
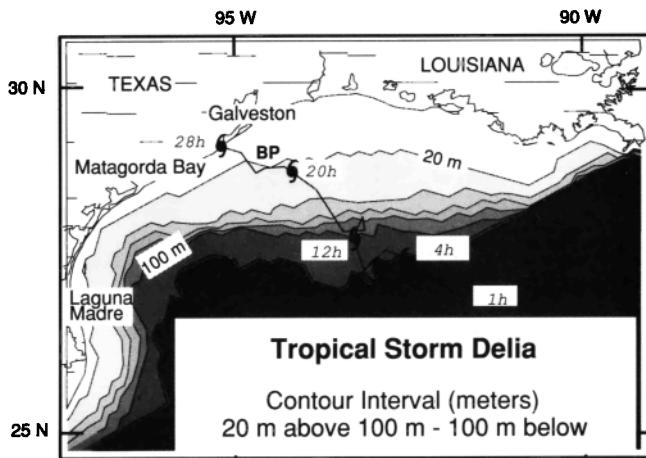
Fig. 4. Detailed track of Tropical Storm Delia and model bathymetry. Numbers along the storm track are model simulation hours. Hour 1 corresponds to 1800 CDT September 3. The location of Buccaneer platform is indicated by BP.

wave, and boundary layer models were based on the fine-grained sediments and roughness height observed at Buccaneer platform [Forristall et al., 1977].

Four types of seafloor substrate were used for the sediment transport experiments as listed in Table 1. The first two were uniform, the third used distinct sediments for the inner and middle/outer shelf regions, and size distribution 4 was an approximation of the fine sand, medium silt, and mud found on the modern Texas-Louisiana shelf (Figure 5). Ten size classes of 1 φ width were used for all sediment distributions, with the percent of sediment within each class determined from the means and standard deviations given in Table 1 using an error function.

4. RESULTS

Wind, circulation, wave, and bed shear velocity fields are shown for simulation hours 4, 20, and 28. These snapshots represent the early, full strength, and late stages of the storm's passage. Only the horizontal currents calculated for the uppermost level (depth 5 m) are presented, because inspection of model output showed that the horizontal circulation field over the shelf varied little in the vertical. Bottom shear velocities are presented for only one substrate (sediment distribution 1), even though they are expected to vary with bottom textures. However, the differences are not significant enough to change the following discussion. Finally, although sedimentation was computed for each hour, the presentation has been simplified to show only the final results.

4.1. Shelf Circulation

Vectors in the northeastern quadrant of Delia's wind field paralleled the Louisiana-Texas coastline by hour 4 of the simulation, with easterly winds of 15 m/s along the coast and speeds in excess of 20 m/s over deeper water (Figure 6a). In response to this wind field, a shelf-wide westward longshore flow was established from eastern Louisiana to Galveston, with a peak speed of 108 cm/s in 10-m water depths (Figure 6b). Coincident with this flow, a forced Kelvin wave developed west of New Orleans (Figure 6c).

Over the next 16 hours, maximum wind speeds increased to 28 m/s. Winds were approximately parallel to the coast throughout much of this interval, but by hour 20 the maximum winds were parallel to shore only along the central Texas coast (Figure 7a). Shelf flows responded such that the previous pattern shifted west-

ward and onshore flow along central Louisiana increased to about 50 cm/s (Figure 7b). Longshore currents exceeded 200 cm/s at this time, with an offshore component from Galveston southward. Flow strength rapidly decreased in the deep water between Matagorda Bay and Corpus Christi (Figure 7b). The limited movement of the eye between hours 3 and 14 and the scale and shape matching between the storm and coastline were responsible for the growth of a forced Kelvin wave along the Louisiana shoreline. By hour 20 the wind had shifted sufficiently to stall this wave, and the predicted coastal setup peaked at 180 cm at Galveston (Figure 7c).

An observed storm surge of 130 cm at Galveston preceded peak currents, and a maximum in excess of 200 cm was recorded 30 hours after landfall, by which time currents had decreased significantly [Morton, 1981]. The coastal setup coincident with the peak currents at Galveston, therefore, fell between these values. The maximum modeled setup (180 cm) in Figure 7c approximately coincides with peak model-hindcast currents, a temporal relationship suggested by the tidal data from Galveston. However, since no model results were produced after landfall, these results cannot be compared to those of Morton [1981] for the interval when coastal setup reached a maximum.

When the eye made landfall at hour 28, the storm winds had fallen to less than 20 m/s everywhere (Figure 8a) and had shifted from predominately shore parallel to shore normal over the shelf. As the wind shifted out of phase with the inertial currents, the hor-

TABLE 1. Textural Data for Event Bed Simulations

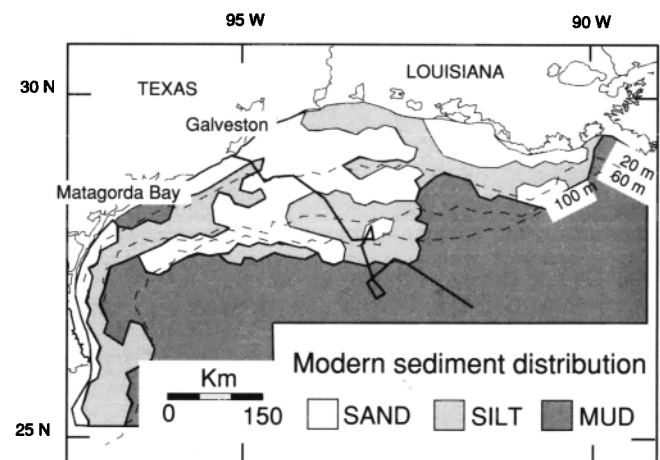| Run	Sediment Distribution	Mean φ	S. D. φ
1	medium silt	5.5	1.0
2	fine sand	2.5	0.8
3	mud line at 20 m		
	inner shelf	2.5	0.5
	middle/outer shelf	7.5	1.0
4	modern sediments		
	nearshore sands	2.5	0.8
	outer shelf muds	7.5	1.0
	mixture	5.5	1.0

Fig. 5. Sediment distribution for the modern northwestern Gulf of Mexico (original data from Curray [1960]); see Table 1 for details. The path of Tropical Storm Delia is represented by the heavy irregular line.
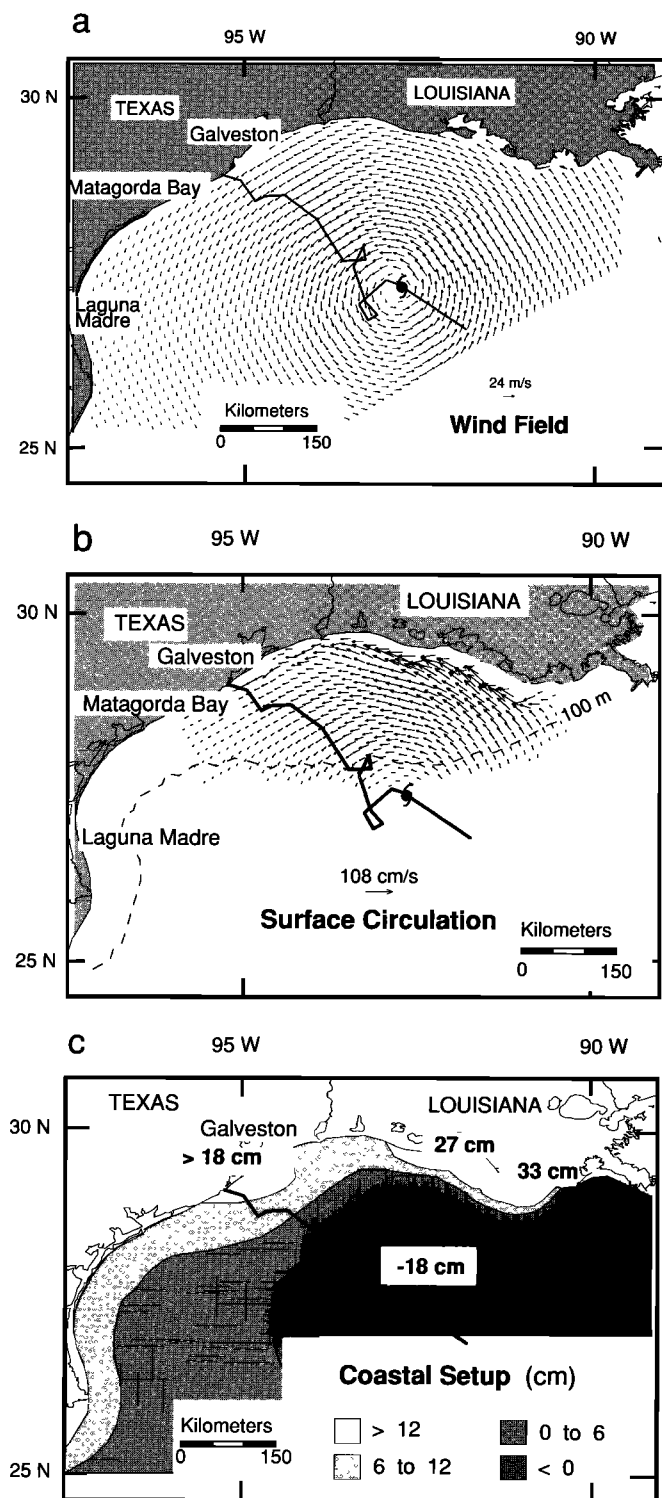
Fig. 6. Simulation hour 4 (2100 CDT September 3): (a) vector plot of wind field, (b) vector plot of the horizontal circulation field within the upper model level (the scale arrow is the largest vector present), and (c) contour plot of the water surface elevation (in centimeters) with respect to still water level. High and low values are labeled. The position of the storm eye is marked by the closed tropical storm symbol.
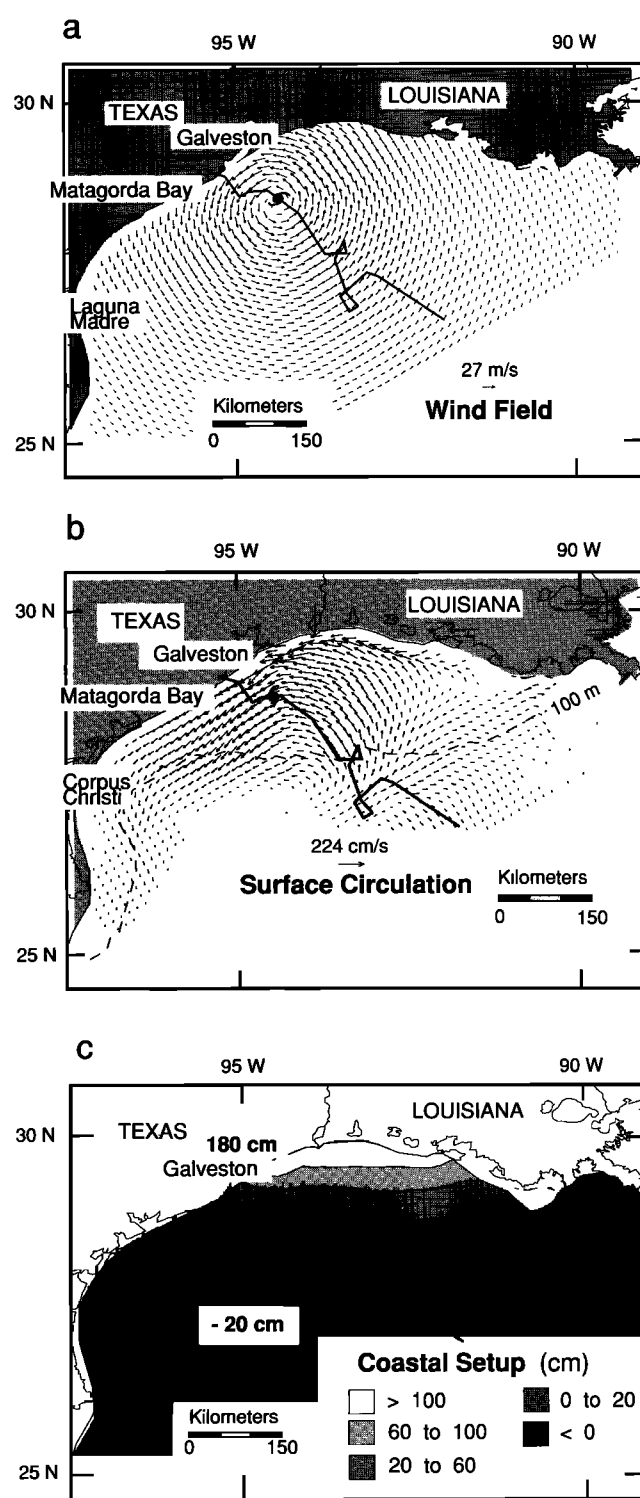
Fig. 7. Simulation hour 20 (1300 CDT September 4): (a) vector plot of wind field, (b) vector plot of the horizontal circulation field within the upper model level (the scale arrow is the largest vector present), and (c) contour plot of the water surface elevation (in centimeters) with respect to still water level. High and low values are labeled. The position of the storm eye is marked by the closed tropical storm symbol.

izontal circulation became dominated by the pressure gradient and inertial oscillations (Figure 8b), and coastal setup at Galveston (Figure 8c) drove adjustment currents as high as 127 cm/s to the southwest and offshore over the Texas shelf. Lower setup near Corpus Christi also generated longshore currents to the south with

magnitudes of approximately 30 cm/s. In direct contrast, convergence between offshore flow and onshore inertial currents over the Louisiana shelf caused a reversal in longshore flow vectors and flow back to the southeast.

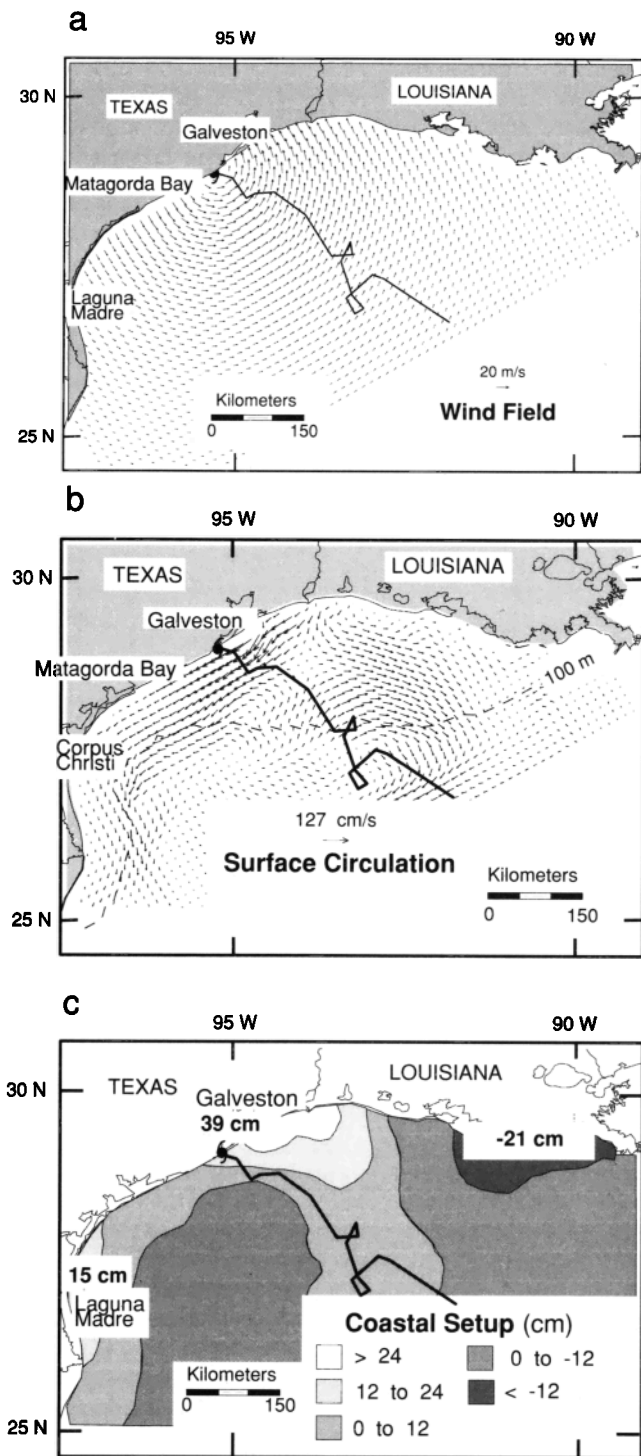The accuracy of the hindcast currents can be estimated at one

Fig. 8. Simulation hour 28 (2100 CDT September 4): (*a*) vector plot of wind field, (*b*) vector plot of the horizontal circulation field within the upper model level (the scale arrow is the largest vector present), and (*c*) contour plot of the water surface elevation (in centimeters) with respect to still water level. High and low values are labeled. The position of the storm eye is marked by the closed tropical storm symbol.

point along the storm path using the data of *Forristall et al.* [1977] (Figure 9). Hindcast surface currents at Buccaneer platform match the observed currents reasonably well until Delia's eye passed Buccaneer at hour 23, when the local currents became too complex to be resolved by the model grid.

4.2. Wind-Wave Field

Landward of the 20-m isobath, $H_{1/3}$ never exceeded 4 m beneath the storm and was more often closer to 3 m (Figure 10). Between 20 and 100 m it ranged from 4 to 10 m, with higher amplitudes near the eye. At water depths greater than 100 m, $H_{1/3}$ remained above 7 m and climbed as high as 30 m. When the eye was over the outer shelf, maximum $H_{1/3}$ coincided with the radius of maximum winds about 80 km from the eye, and as it moved onto the inner shelf, high waves endured offshore because of high winds, a large fetch, and greater water depths.

Before hour 20, θ_o paralleled the coast from New Orleans to Galveston and was approximately collinear with longshore currents (compare Figures 10*a* and 10*b* with Figures 6*b* and 7*b*). However, as Delia's eye approached landfall, θ_o to the right of the storm track underwent a clockwise rotation and to the left an anticlockwise rotation, causing waves near the coast to travel at high angles to longshore currents (Figure 10*c*).

The accuracy of the computed wave field near the storm path can be evaluated using time series of significant wave heights and wave energy spectra at Buccaneer. Model-calculated values of $H_{1/3}$ do not compare well with those observed by *Forristall et al.* [1978], being too low by about 0.5 m during the approach of the storm and 1 m at the peak (Figure 11). A probable cause can be inferred from a comparison of model and measured spectra for the peak of the storm (Figure 12). Although the model predicted the wind sea portion of the spectrum reasonably well, there is an obvious low-frequency component in the confused seas which existed at that time. This was not expected from the preliminary comparisons presented in Appendix B.

4.3. Combined Wave-Current Shear Velocities

The benthic boundary layer model calculates the combined shear stresses at the seafloor, thereby allowing the bed shear velocity, $u_* = \sqrt{\tau_o/\rho}$, to be found. Variations in u_* can be subdivided into three periods during the storm's passage: (1) an early phase prior to hour 4, (2) an intermediate period between hours 5 and 20, and (3) a waning phase as the storm approaches landfall after hour 24.

Prior to hour 4, u_* was everywhere less than about 8 cm/s (Figure 13*a*). Values of 2 cm/s covered the shelf out to the 80-m iso-
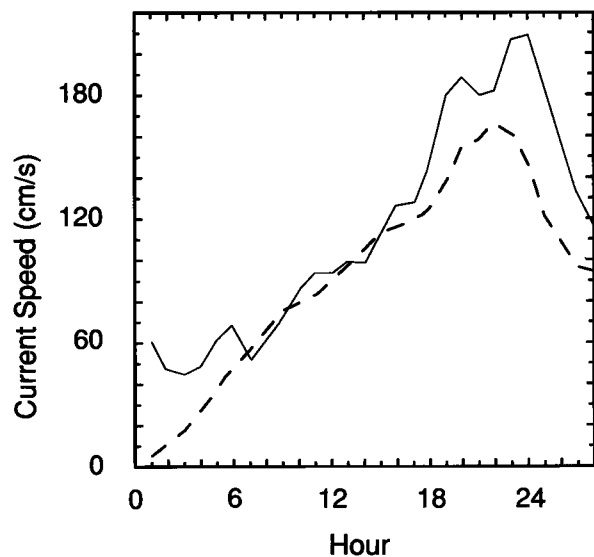

Fig. 9. Surface currents at Buccaneer platform. The solid line represents the data measured by *Forristall et al.* [1977], and the dashed line is model output.
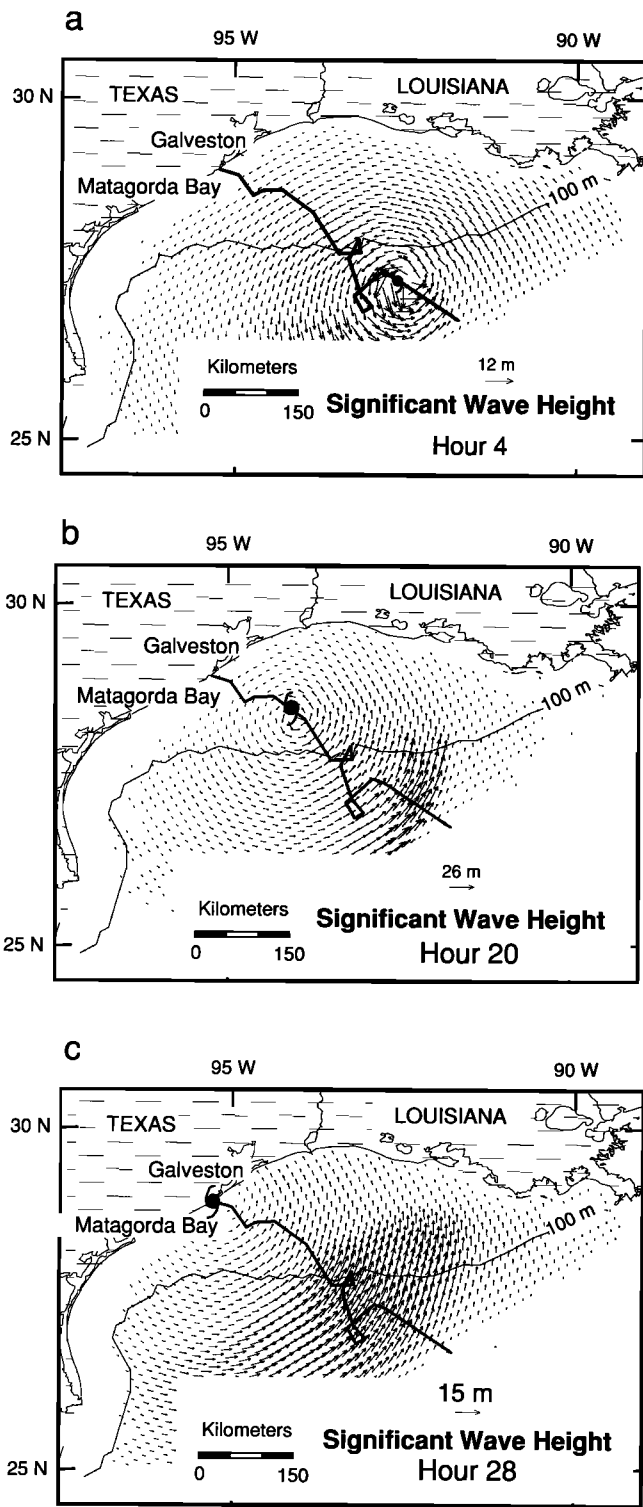
a

b

c

Fig. 10. Vector representation of significant wave field at (a) hour 4, (b) hour 20, and (c) hour 28. $H_{1/3}$ is proportional to the length of the arrows, and the direction of wave propagation θ_o, is the vector direction. The vector scale is the maximum present on the plot.

bath from eastern Louisiana to Matagorda Bay, with maxima occupying a shore-parallel band along central Louisiana in water less than 20 m deep. Currents and waves during this period were both westerly along the entire Louisiana coast with peaks of 1 m/s (Figure 6b) and 1 to 2 m (Figure 10a), respectively, along eastern Louisiana.

Hours 5 to 12 mark a transition period as a second region of elevated shear velocities developed landward of the 20-m isobath and magnitudes increased over much of the Louisiana shelf (Figure 13b). This isobathyal form partly results from the discretization of bathymetry into 10-m levels. The nearshore region of elevated shear velocities also shifted westward during this interval and increased to more than 8 cm/s. The causes of this westward and offshore shift in u_* isopleths can be seen in Figures 7b and 10b. As Delia's eye crossed the shelf, coastal currents generated by wind stress and coastal setup increased and were collinear with θ_o. The remainder of the intermediate stage was characterized by consolidation of the offshore high into a bull's-eye between 20- and 40-m water depths with an increase in the maximum to 24 cm/s and values exceeding 6 cm/s from central Louisiana to Galveston (Figure 13c). This pattern reflects the further intensification of the storm circulation with approaching landfall, as coastal currents exceeded
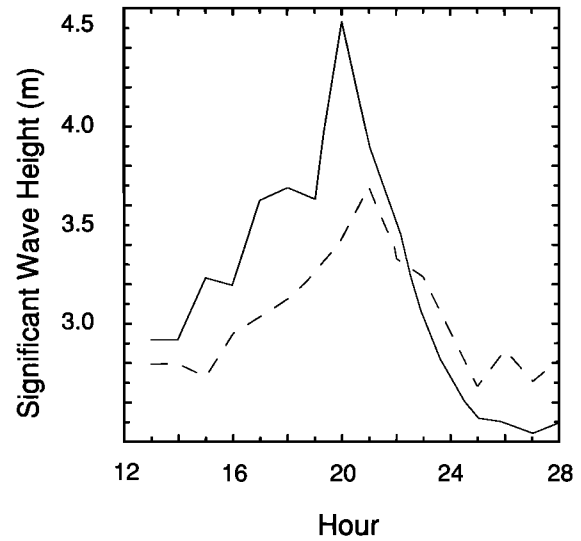

Fig. 11. Observed (solid line) [from Forristall et al., 1978] versus predicted (dashed line) significant wave heights $H_{1/3}$ at Buccaneer platform.
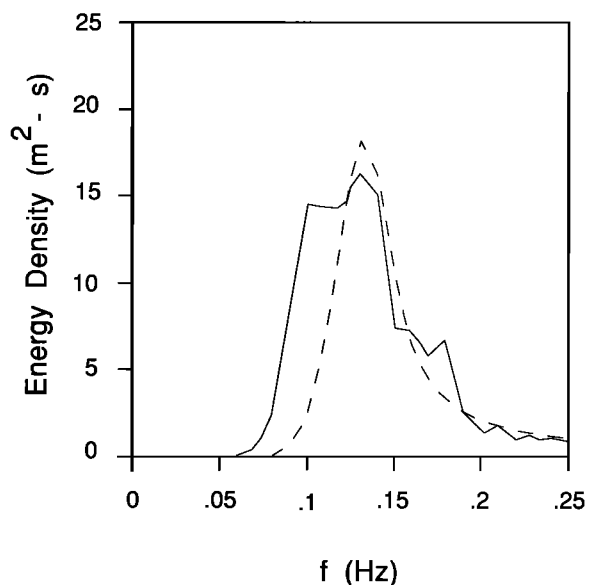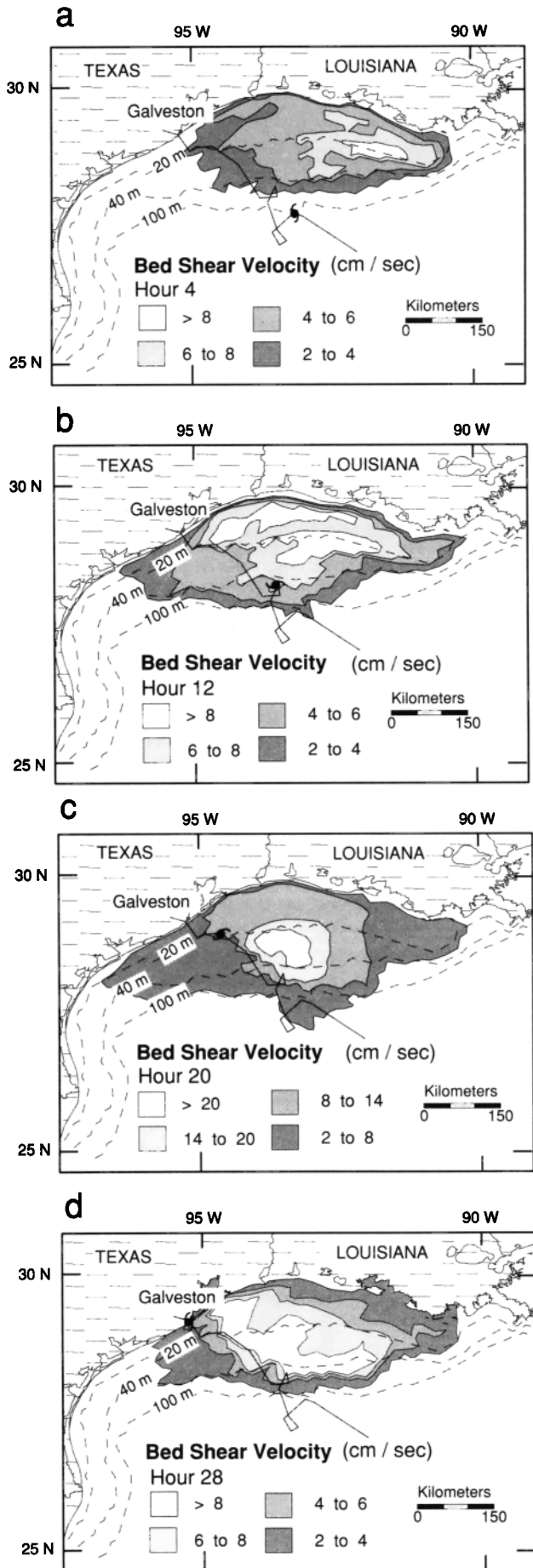

Fig. 12. Model spectrum (dashed line) and calculated spectrum using steady current interaction (solid line) from Buccaneer at hour 18 [from Forristall et al., 1978].

1 m/s over much of the northwestern shelf (Figure 7b) and winds were strong enough to generate high seas across a range of water depths (Figure 10b).

During the final stage, from hours 21 to 28, the maximum shear velocity decreased to 16 cm/s (Figure 13d). By hour 28 the 8-cm/s isopleth formed a tongue attached to the Texas coast at Galveston, extending southeast to the 80-m contour. This tongue was created by setup-driven longshore currents greater than 120 cm/s (Figure 8b) and significant wave heights in excess of 4 m.

4.4. Character of Delia's Event Bed

Delia's event bed is evaluated using final values for the sediment parameters from Figure 5. Erosion depth $D_E(x, y)$ is defined as the maximum depth of erosion into the seafloor during the course of the storm and is always negative. Seafloor elevation $H_{sf}(x, y, t)$ is the height of the seafloor at any time relative to its initial value. It may be negative or positive, depending on whether net erosion or deposition occurs at a grid point. $H_{sf} - D_E$ defines $T_S(x, y)$, the event bed thickness which is either zero or positive. The cumulative volumetric median size of the sediment deposited at a grid point is $D_{50}(x, y)$.

Size distribution 1: Medium silt. Sea floor erosion occurred to the right of the storm track and followed bathymetric contours (Figure 14a), partly because of the steps in the model bathymetry. D_E exceeds 60 cm between the 60- and 100-m isobaths within an area roughly 75 km in length and 50 km in width. Sediment removed from these areas was typically deposited within 50 km to the west, resulting in an irregular seafloor elevation pattern (Figure 14b). Sediment removed from the deep scour hole between the 40- and 100-m isobaths was deposited partly as a thin blanket (< 5 cm) and partly as an arcuate bed. Net erosion and deposition alternate along the 30-m isobath with transport distances on the order of 20 km.

T_S exceeds 40 cm to the right of the storm track in water depths of 60 m (Figure 14c). The event bed thins laterally, is irregular and discontinuous shoreward, and terminates abruptly to the southwest. The median grain size of the bed is uniform and finer than 5φ (0.031 mm) because of the ready availability of clay within the initial sediment distribution. The bed is coarsest along the northeastern Texas coast where D_{50} is approximately 5.6 φ (0.02 mm). This resulted from the landward boundary condition which introduced sand-sized sediment only. Mixing of this sand with the fine sediment transported by the storm currents produced intermediate values of D_{50}.

Size distribution 2: Fine sand. The sandy sediment of the second experiment significantly limited erosion away from the storm track (Figure 15a). D_E attains a maximum of 100 cm to the right of the storm track in water deeper than 80 m, with much lower magnitudes scattered in shallower water, wherever local bed shear gradients were sufficient to entrain the finer sediment. The predicted distribution of H_{sf} for this experiment is much simpler than in the previous case because of reduced transport. Areas of deposition are more closely associated with erosion, and sedimentation is confined to the storm track and coastline (Figure 15b). This simpler topography is a function of sediment availability. The finest grain size is 4.5 φ (0.044 mm), coarse enough to severely limit the suspended sediment load. Thus, the resulting transport pattern

Fig. 13. Contour plots of bed shear velocities u_* at (a) hour 4, (b) hour 12, (c) hour 20, and (d) hour 28. The contour interval in Figures 13a, 13b, and 13d is 2 cm/s. In Figure 13c it is 6 cm/s. The position of the storm eye is marked by the closed tropical storm symbol.
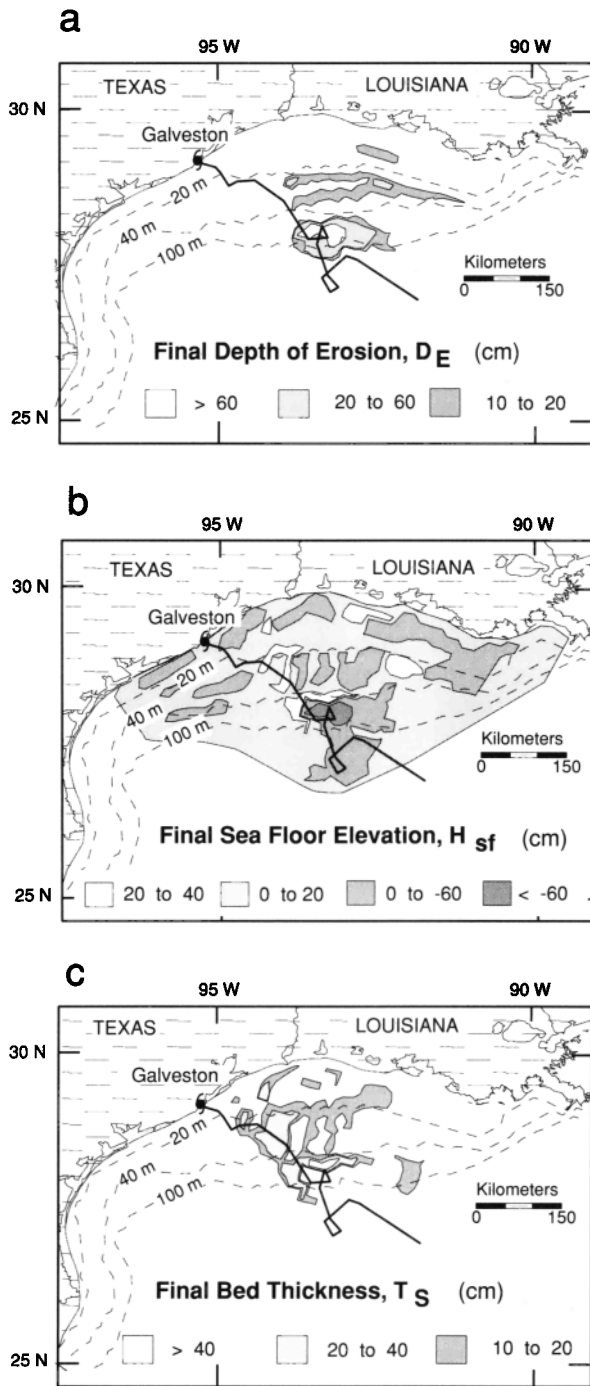
Fig. 14. Contour plots of (a) final erosion depth D_E, (b) seafloor elevation H_{sf}, and (c) storm bed thickness T_S for the uniform-silt initial sediment distribution at hour 28. The contour intervals are variable with values given by the key.
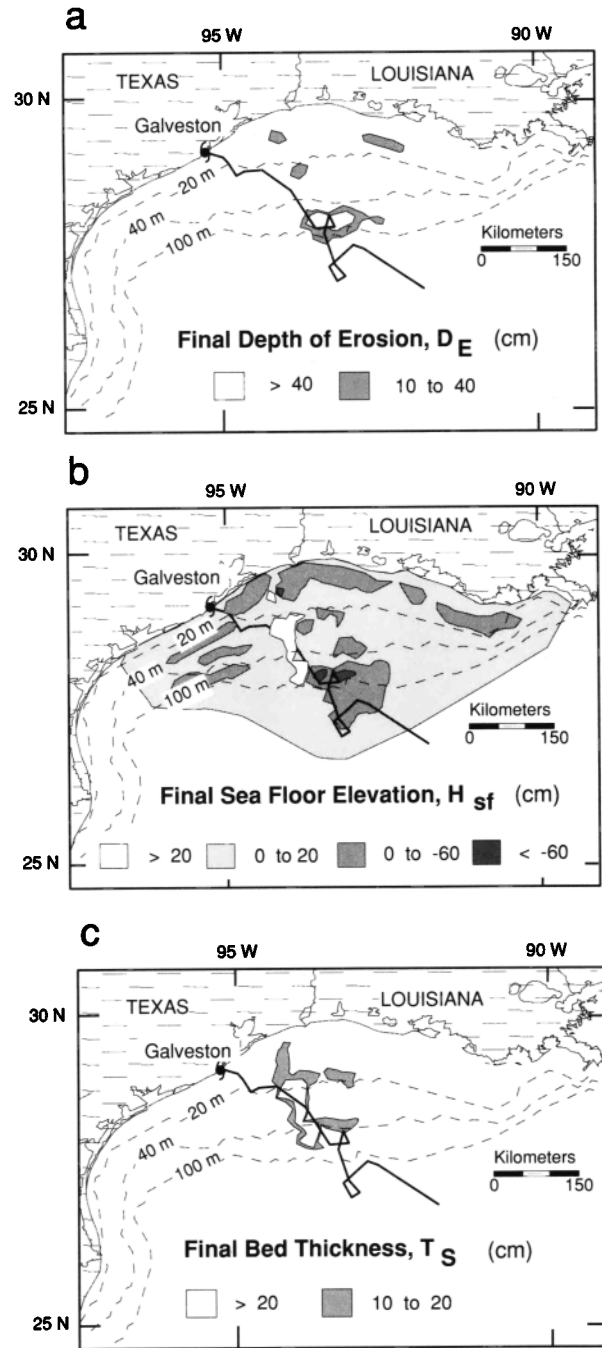

Fig. 15. Contour plots of (a) final erosion depth D_E, (b) seafloor elevation H_{sf}, and (c) storm bed thickness T_S for the uniform-sand initial sediment distribution at hour 28.

reflects the concentration of u_* gradients near the center of the storm (Figure 13c) and along the coastline (Figure 13d).

The thickest event bed is located along the storm path and terminates east of Galveston (Figure 15c). It averages 20 cm in thickness and attains a maximum of 40 cm in water depths of 40 to 60 m. The thickness of coastal sediments increases westward from 0.6 cm along the central Louisiana coast to about 1.9 cm midway between the Texas-Louisiana border and Galveston. However, this feature only becomes visible in Figure 15c when its thickness exceeds the contour interval of 10 cm. D_{50} ranges from 5 to 4 φ

(0.03 to 0.06 mm) for the thickest part of the event bed. The sediment deposited along the coast reflects the introduction of sand at the landward boundary: D_{50} ranges from 3.6 φ (0.08 mm) in the east to 3.3 φ (0.1 mm) in western Louisiana and reaches a high of 1.27 φ (0.28 mm) near Galveston. The trend reflects the increasing offshore component of the longshore currents.

Size distribution 3: Mud line at the 20-m isobath. The sedimentation pattern for this experiment is not simply a combination of previous results, because the nearshore sands in this sediment distribution were better sorted than the uniform sand used in the second experiment and the offshore mud was finer than in the first experiment (see Table 1). D_E is distributed similarly to the uniform

silt case for water deeper than 30 m (Figure 16a), except for the conspicuous lack of erosion along the 30-m isobath. This difference can be explained by the timing of maximum bed shear stresses. Most erosion occurred after hour 16, when u_* peaked and currents flowed onshore south of Louisiana (Figure 7b). These currents crossed the mud line and entered a part of the shelf where only sand was present in the bed; thus there was no transport of sediment finer than sand landward of the mud line, and, since there was no downflow transport, there could be no erosion immediately seaward either, as indicated by (4). The main depocenter resembles those of the previous experiments (Figure 16b). Alternating erosion and deposition are indicated along the 30-m isobath, and, as before, H_{sf} increases systematically to the west along the Louisiana coast.

The distribution of T_S (Figure 16c) is similar to the uniform-sand experiment for water depths greater than 40 m, but between 20 and 40 m the event bed takes on the character of a ragged blanket. Shoreward of the 20-m isobath the bed thickens, reflecting coarser sediment transported offshore. The textural characteristics of the event bed can be evaluated in terms of the volumetric percent of sand (4 to -1 φ) and silt (8 to 4 φ). Beyond the mud line, the event bed averages about 60% silt by volume for much of its extent (Figure 17a). This is mostly the very fine silt of the muddy offshore sediment. Near the 20-m isobath, silt is mixed with sand (Figure 17b), and in shallower water, tongues of silt-free sand originate from the shoreface, transported by either weak jets (Figure 8b) or pressure-driven adjustment currents.

Size distribution 4: Modern sediments. Scour exceeds 20 cm in three areas where the initial substrate was silt ($\mu = 5.5$ φ) (Figure 18a), with the deepest erosion located as in the previous experiments because of large u_* gradients and the availability of finer sediment. A second area located along the 30-m isobath lies astride the boundary between the initial mud ($\mu = 7.5$ φ) and silt substrates. A third area is present along the coast in 20 m depths with a silt substrate. The isobathyal character and distance from the coast indicate that this erosion resulted from longshore currents rather than offshore adjustment currents.

The resulting distribution of H_{sf} (Figure 18b) is more complex than in previous experiments because of the availability of a range of sediment sizes at all water depths. Positive H_{sf} is found in initially sandy sediment over a broad area, and because no significant erosion is indicated for this substrate (Figure 18a), this deposition resulted from transport of finer sediment from adjacent areas. Despite the use of three initial sediment distributions for this experiment, the results for bed thickness are not significantly different from previous runs in which sufficient fine material was available (compare Figures 16c and 18c). The main difference is the greater volume of silt deposited adjacent to the coastline because of availability. In water depths over 40 m, D_{50} is about 9.5 φ (0.0014 mm), whereas between the 40- and 20-m isobaths, it increases to about 5.7 φ (0.02 mm). Along the eastern Louisiana-western Texas coast it averages 3.3 φ (0.1 mm).

5. DISCUSSION

5.1. Uncertainties in Model Results

The relative error of the results for wind speed, significant wave height, and currents can be assessed by comparing the computed values to those observed at Buccaneer platform (Figure 19). Positive errors indicate underprediction of a parameter. Errors for wind speed remain below 20% until hour 20 when the eye passed over Buccaneer, at which time they become strongly negative. This
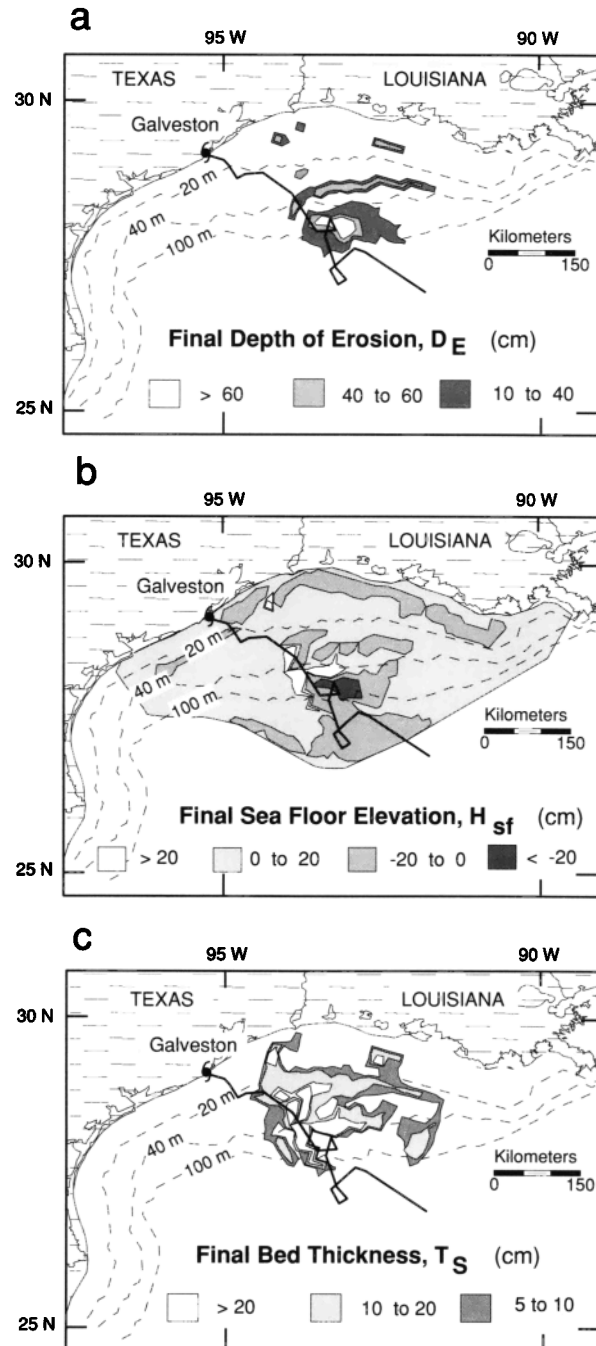
Fig. 16. Contour plots of (a) final erosion depth D_E, (b) seafloor elevation H_{sf}, and (c) storm bed thickness T_S for the initial sediment distribution with a mud line at the 20-m isobath for hour 28.

reflects the inability of the simple wind model to account for winds within the eye and as the storm breaks up. As suggested by Figure 11, $H_{1/3}$ is underestimated before the maximum of the storm and overestimated afterward. The bottom currents are better predicted after the storm peak than were the surface currents (Figure 9) because of the decrease in wind stress as a driving force. The errors indicate that model results are not usable before hour 6 because the circulation model had not reached dynamical equilibrium before then. However, for the period of greatest storm effects at Buccaneer the separate components of S^3 appear reasonably accurate.

The effects of these relative errors on the calculation of the sea-

a

Percent Silt in Storm Bed
Mud Line at the 20 m Isobath

> 60 ⃞　40 to 60 ⃞　20 to 40 ▨

b

Percent Sand in Storm Bed
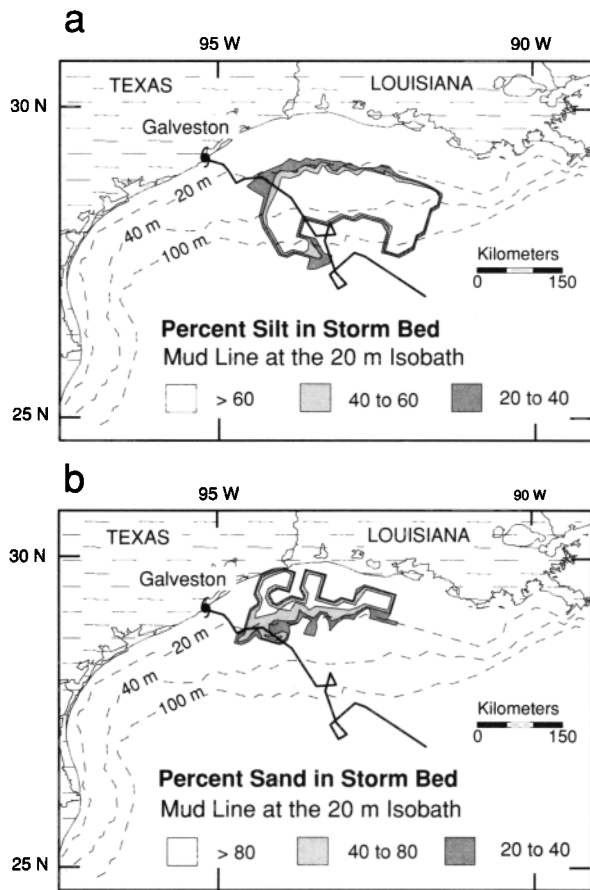Mud Line at the 20 m Isobath

> 80 ⃞　40 to 80 ⃞　20 to 40 ▨

Fig. 17. Contour plots of the volumetric percent of the coarse fraction within the inner shelf storm bed at hour 28 for the initial sediment distribution with a mud line at the 20-m isobath. (a) Silt fraction (8 to 4 φ). (b) Sand fraction (4 to -1 φ).

floor stresses can be estimated following the method used by *Lyne et al.* [1990]. For independent small errors in the current speed U_r, bottom roughness parameter z_o, bottom wave orbital amplitude A_b, and wave period T, the uncertainty in the current shear velocity u_{*c} can be estimated from

$$\frac{\Delta u_{c^*}}{u_{c^*}} = \frac{\left[\frac{\Delta U_r}{U_r} + F_{zo}\frac{\Delta z_o}{z_o} + F_A\frac{\Delta A_b}{A_b} - F_T\frac{\Delta T}{T}\right]}{(1+F_R)} \tag{5}$$

where the coefficients F_{zo}, F_A, F_T, and F_R are defined by Lyne et al., and can be calculated from boundary layer model parameters. We will neglect uncertainties in z_o because of the difficulty of estimating them and the order-of-magnitude decrease in the F_{zo} term [*Lyne et al.*, 1990]. Using the output for hour 18 for Buccaneer (during the peak of the storm), $F_A = 0.489$, $F_T = 0.422$, and $(1+F_R) = 1.422$. The uncertainties can be taken from Figure 19 and found from linear wave theory: $\Delta U_r/U_r = -0.019$, $\Delta A_b/A_b = 0.289$, and $\Delta T/T = 0.053$. Inserting these values in (5) gives an estimate of the dimensionless relative error for u_{*c}, in this case 0.07. The uncertainty in A_b has the greatest effect but the other terms in (5) are of similar magnitude and cancel for this example.

5.2. Vertical Structure of Coastal Storm Currents

The present conceptual model of event bed genesis, well summarized by *Duke et al.* [1991], calls for wind-driven longshore currents to be acted upon by a cross-stream Coriolis force.
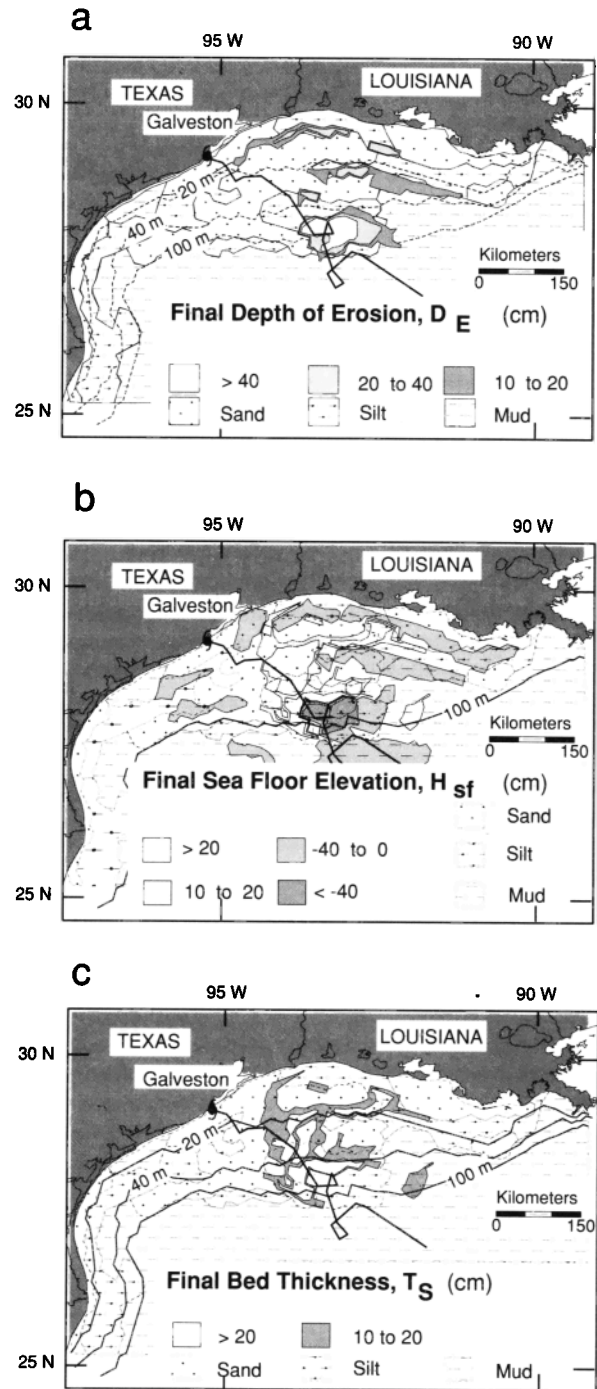
a

Final Depth of Erosion, D $_E$ (cm)

> 40 ⃞　20 to 40 ⃞　10 to 20 ▨
Sand ⃞　Silt ⃞　Mud ⃞

b

Final Sea Floor Elevation, H $_{sf}$ (cm)

Sand
> 20 ⃞　-40 to 0 ⃞　Silt
10 to 20 ⃞　< -40 ▨　Mud

c

Final Bed Thickness, T$_S$ (cm)

> 20 ⃞　10 to 20 ▨
Sand ⃞　Silt ⃞　Mud ⃞

Fig. 18. Contour plots of (a) final erosion depth D_E, (b) seafloor elevation H_{sf}, and (c) storm bed thickness T_S for the initial sediment distribution based on the modern sediments for hour 28. The overlay of sediment type shows the relationship between initial substrate and sedimentation.

Through coastal setup this force comes to be balanced by a cross-shelf pressure force that generates shore-oblique, downwelling bottom currents. These bottom currents interact with wave orbital bottom motions to transport sand from the shoreface obliquely seaward and along shore. Inherent in this conceptual model is a critical assumption concerning the structure of the shelf currents under storms. As water depth increases seaward, it is assumed that overlap of an upper and lower boundary layer decreases and a friction-dominated zone is replaced by a transition zone that reflects both bed friction and geostrophy. Still further offshore, in water depths
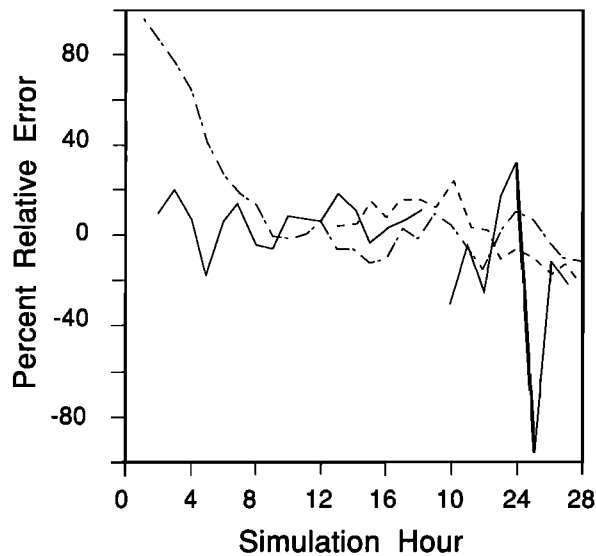
Fig. 19. Percent relative error for wind speed (solid line), steady bottom currents (dash-dotted line), and significant wave height (dashed line) at Buccaneer.

great enough for the two boundary layers to separate, a core flow is assumed to develop where pure geostrophy operates [*Swift and Niedoroda*, 1985].

The hindcasts presented here do not show this structure under the storm. Rather, because of a deepened wind-mixed layer, the upper and lower boundary layers overlap, upper and lower Ekman veering cancel to varying degrees, and shelf flow at all levels is primarily in the wind direction. No appreciable coastal downwelling occurs under the storm. The thickness of the wind-mixed layer calculated in the model for the moderate winds of Delia is about 50 m, placing most of the Texas-Louisiana shelf within the friction-dominated zone. This is consistent with observations from deep-sea buoys [e.g., *Martin*, 1982; *Sanford et al.*, 1987], hydrographic profiles [*Ichiye*, 1972], and other numerical results [*Cooper and Thompson*, 1989] wherein depths of the wind-mixed layer are also on the order of 50 m.

Previous attempts to understand hurricane sedimentation on the Texas coast [*Nummedal and Snedden*, 1987; *Morton*, 1988; *Snedden et al.*, 1988; *Snedden and Nummedal*, 1990] have invoked a geostrophic structure for the shelf flow, including downwelling. In contrast, we conclude that the mixed-layer depth under storms may commonly exceed local water depth, thereby causing overlap between the upper and lower friction layers. This suggests that for shallow water (less than 30 m) the ebb-flow model of *Hayes* [1967] may be appropriate. Of course, away from the storm center where winds decrease, or in heavily stratified waters, the present conceptual model may still be applicable.

5.3. Storm Sedimentation Patterns

These numerical experiments demonstrate that a moderate storm such as Tropical Storm Delia can produce a regionally extensive scour surface confined for the most part to the right of the storm track. When a mud line is present, as in the third experiment, up to 60 cm of scour is predicted in water depths of 40 to 80 m. Above this scour surface, an event bed of more than 20-cm thickness may remain after the storm's passage, consisting of sand landward and finer-grained sediments seaward of the mud line. Contrary to conventional wisdom, the bulk of the predicted bed is deposited in water depths greater than 20 m, even for the sandy substrate. When

finer sediment is present, this depth increases to as much as 80 m as a result of landward transport of mud. Although entrainment of this finer sediment is overpredicted, this pattern is considered robust because of the similar pattern for sand.

Two sedimentation regimes are apparent in the hindcasts, one shallow (less than 40 m) and one deep (greater than 40 m). Notably, most field data have been collected within the shallow regime [e.g., *Hayes*, 1967; *Snedden et al.*, 1988; *Gagan et al.*, 1990]. Within both regimes the computed sediment transport is primarily in the form of suspended load, so that the direction of transport is parallel to steady currents. Because of the restraining influence of the coastline, currents within the shallow regime are parallel to shore throughout Delia's passage, with a slight offshore component adjacent to the coast. Thus, suspended sediment transport within this regime results from wind- and pressure-driven flows directly associated with the longshore wind stress. Deposition occurs along the coast as a result of adjustment currents with an offshore component. Sediment transport paths within the deep regime vary more, because there is no constraining coastline. Currents rotate by as much as 180° during Delia's passage. This rotation is caused by both the changing wind stress (rotating clockwise) and the Coriolis force acting on deepwater inertial currents. Sediments transported by these currents to the right of the storm path were carried westward during the first part of the storm and landward later.

The importance of waves in resuspending sediment during a storm event has been investigated on a basin scale by *Graber et al.* [1989] for the East China and Yellow seas. Because of the limited fetch within these enclosed seas, wave heights were restricted for all water depths. Nevertheless, the critical shear stress for medium to fine sand was exceeded in water depths as great as 60 m for several hours. The largest shear velocities occurred in water depths of 22 m where computed values approached 5.3 cm/s. This is considerably less than the >20 cm/s seen in Figure 13c but the cross-shelf distribution is similar. Of course, this study uses steady currents as well as waves to compute combined shear stresses, and the wind field is much stronger. The importance of including the wave field in computing seafloor stresses is seen when they are excluded (Figure 20). The shear velocities have decreased to about 6 cm/s near the coast, and the maximum bed thickness is less than 0.5 mm.

A comparison of the hindcast bed with the observed Delia bed would be desirable, but sedimentological data on this bed are scarce. *Morton* [1988] discussed the textures of surface sediment samples collected near Buccaneer one year after Delia. High concentrations of sand (> 75%) occurred in shore-parallel linear bars several kilometers in length. Although features at this scale are not resolved in the simulations, the model does predict high sand content in the area studied by Morton in a bed up to 10 cm thick. *Snedden et al.* [1988] discuss the distribution of sandy and silty layers within sediments inferred to have been deposited by Hurricane Carla in water shallower than 50 m on the south Texas coast. Between the 20- and 30-m isobaths, they measured a sandy bed with a maximum thickness of 6 cm. This is comparable to the event bed deposited near the Texas-Louisiana border for the mud line sediment distribution discussed in this study.

It is also encouraging that several characteristics of the storm bed hindcast in this study are comparable to the bed produced by Cyclone Winifred off the northeast Australia coast [*Gagan et al.*, 1990]. The greatest erosion in each case occurs in midshelf water depths, presumably because of the increased efficiency of storm waves in entraining sediment there. The magnitudes of erosion predicted by the transport model are much greater, however,
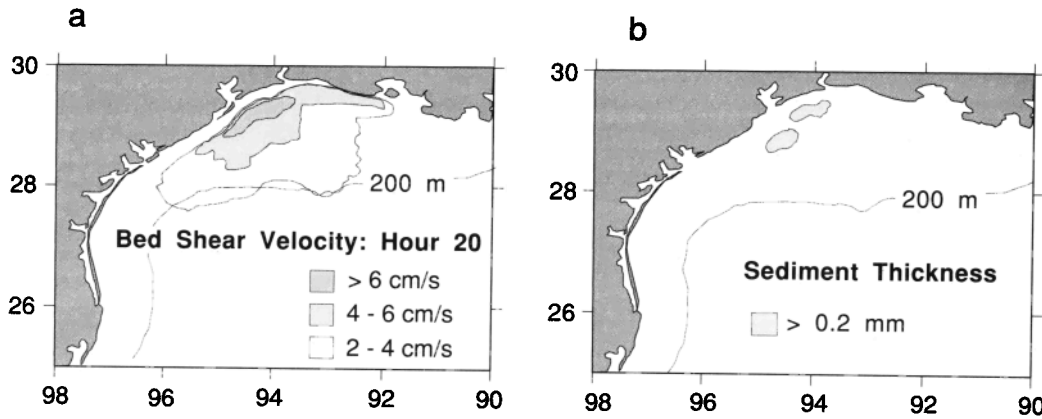
a

b

Fig. 20. Contour plots of (a) bed shear velocity at hour 20 and (b) final sediment thickness for seafloor stresses computed using only steady currents from the circulation model.

because cohesion, bed armoring, and grain hiding are neglected. The Winifred bed consists of silty-sandy sediment from the coast transported tens of kilometers offshore and significant quantities of midshelf mud transported a similar distance shoreward. This latter mud forms the bulk of the Winifred bed, just as predicted in the Delia simulations. Also, resuspension and settling on the inner Australian shelf produced a recognizable storm bed even where sediment transport was minor.

6. CONCLUSIONS

We have attempted to define the generative mechanisms, spatial scales, and textural characteristics of event beds produced by tropical cyclones using a Storm Sedimentation System which includes (1) a hurricane wind field, (2) a three-dimensional ocean circulation model, (3) a finite-depth wind sea model, (4) a combined wave-current benthic boundary layer model, (5) a sediment transport model and (6) a bed conservation model.

The results are considered to be first approximations only because there is no coupling between system components representing processes with known feedback, and the assumption of a uniformly homogeneous water column everywhere is not fully justified. Further, wind waves in shallow water are systematically underpredicted, because the swell component of the wind-wave field is neglected. Several factors affecting entrainment of fine-grained sediment are ignored, such as bed armoring, cohesion, and grain hiding. Finally, the simple cyclonic wind field algorithm used herein is not adequate far from the storm eye and cannot capture atmospheric processes preceding arrival of the storm at the shelf or after landfall.

The system is used to hindcast ocean circulation and sedimentation during Tropical Storm Delia, a moderate storm which passed over the Texas-Louisiana continental shelf. In water deep enough for high storm waves (greater than 40 m), combined flows transport sediment along-shelf and shoreward. In water depths of 20 to 40 m, currents transport sediment along the shelf, diffusing it over a wide area. Along the coast, adjustment currents driven by the pressure gradient locally transport shoreface sand offshore no further than the 30-m isobath. The coastal circulation system producing these transport paths is systematically different from that predicted by the mid-latitude geostrophic model, probably because the Coriolis force is reduced at lower latitudes and the wind-mixed layer is thicker. The most significant difference is a lack of coastal downwelling.

The dependence of bed characteristics on initial substrate has been evaluated using four sediment distributions: uniform silt, uni-

form sand, a mud line at the 20-m isobath, and a simplified modern sediment distribution. Generally, it can be said that Delia's event beds in each case are ragged blankets up to 60 cm thick, covering the Texas-Louisiana shelf to the right of the storm track. An unexpected result is significant erosion and deposition seaward of the 40-m isobath for all substrates, although, admittedly, this erosion occurred within finer sediment for which the transport model does not include cohesive effects.

APPENDIX A: THE CIRCULATION MODEL

Ocean circulation for S³ is calculated by the three-dimensional turbulent energy model of *Leendertse et al.* [1973] and *Leendertse and Liu* [1975, 1977, 1978]. It solves the primitive equations for fluid motion in Cartesian coordinates using the f plane approximation. The simplified equations of motion in the x and y directions are, respectively

$$\frac{\partial u}{\partial t} + \frac{\partial (uu)}{\partial x} + \frac{\partial (uv)}{\partial y} + \frac{\partial (uw)}{\partial z} =$$

$$fv - \frac{1}{\rho}\frac{\partial p}{\partial x} + \frac{1}{\rho}\left(\frac{\partial \tau_{xx}}{\partial x} + \frac{\partial \tau_{xy}}{\partial y} + \frac{\partial \tau_{xz}}{\partial z}\right) \quad \text{(A1)}$$

$$\frac{\partial v}{\partial t} + \frac{\partial (vu)}{\partial x} + \frac{\partial (vv)}{\partial y} + \frac{\partial (vw)}{\partial z} =$$

$$-fu - \frac{1}{\rho}\frac{\partial p}{\partial y} + \frac{1}{\rho}\left(\frac{\partial \tau_{yx}}{\partial x} + \frac{\partial \tau_{yy}}{\partial y} + \frac{\partial \tau_{yz}}{\partial z}\right) \quad \text{(A2)}$$

where u, v, and w are components of the velocity vector along the x, y, and z axes; t is time; f is the Coriolis parameter; ρ is seawater density; p is pressure; and τ_{xx}, etc., are components of the Reynolds stresses. The equation of motion in the z direction reduces to

$$\frac{\partial p}{\partial z} + \rho g = 0 \quad \text{(A3)}$$

where g is the acceleration of gravity. For incompressible fluids the equation of continuity is

$$\frac{\partial u}{\partial x} + \frac{\partial v}{\partial y} + \frac{\partial w}{\partial z} = 0 \quad \text{(A4)}$$

Equations (A1) and (A2) have introduced the Reynolds stresses τ_{xx}, etc., which must be related to the velocity field. The horizon-

tal Reynolds stresses are found from the curl of the horizontal circulation field, whereas the vertical components, τ_{xz} and τ_{yz}, are dependent on the vertical eddy viscosity from

$$\tau_{xz} = \frac{\rho A_z u}{h} \qquad (A5)$$

where h is the average thickness of adjacent model levels for which momentum exchange is being computed and A_z is the vertical eddy viscosity, given by

$$A_z = L_o \sqrt{E} \exp(-R_1 R_g) \qquad (A6)$$

where L_o is the mixing length given by $L_o = a_o L_\infty$, L_∞ is the integral-scale mixing length [Niiler, 1982] $L_\infty = \kappa z (1-z/d)^{1/2}$, a_o is a constant with a value of 0.46 [Zilitinkevich et al., 1967], κ is von Karman's constant, z is the depth below the surface, d is the total water depth, E is the subgrid-scale turbulent energy density, R_1 is a constant, and R_g is the gradient Richardson number. The exponential term introduces the effects of density stratification. The equation for τ_{yz} is analogous.

Boundary conditions include (1) no flow at lateral boundaries, (2) a surface stress $\tau_w = \rho C_d U_w^2$, where C_d is the drag coefficient and U_w is the wind speed at 20 m, and (3) a bottom stress $\tau_b = (\rho g u^2)/C^2$, where C is the Chezy coefficient. The Chezy coefficient is found from $C = R^{(0.17)}/n$, where R is the thickness of the lowermost model level present at a grid point and n is Manning's coefficient. This formulation was used in the original model [Leendertse et al., 1973] and was retained because it allowed some variability of bottom friction and the value of n could be approximated from readily available data.

Turbulent energy is calculated from a conservation equation:

$$\frac{\partial E}{\partial t} + \frac{\partial (uE)}{\partial x} + \frac{\partial (vE)}{\partial y} + \frac{\partial (wE)}{\partial z} =$$

$$\frac{\partial}{\partial x}(D_x \frac{\partial E}{\partial x}) + \frac{\partial}{\partial y}(D_y \frac{\partial E}{\partial y}) + \frac{\partial}{\partial z}(\kappa' \frac{\partial E}{\partial z}) + S_E - \xi \qquad (A7)$$

where D_x and D_y are horizontal exchange coefficients found from the curl of the horizontal velocity field. Here, κ' is the vertical exchange coefficient $\kappa' = a_1 A_z$, S_E is a turbulence generation term found from the velocity gradient, and ξ is a dissipation term $\xi = a_2(E^{3/2} / L_o)$. The constants a_1 and a_2 are assigned values of 0.73 and 0.046, respectively [Zilitinkevich et al., 1967].

Because of the generally well mixed nature of the upper ocean over the continental shelf during tropical cyclones, no salinity or temperature gradients were used, and decoupling of the mixed

layer from the deep water was accomplished using the Ekman friction depth [Pond and Pickard, 1983]:

$$D_E = \pi \sqrt{\frac{2A_z}{f}} \qquad (A8)$$

The model is solved on a staggered finite-difference grid using a central difference scheme for both time and space. For a discussion of the finite-difference formulation see Leendertse et al. [1973] and Leendertse and Liu [1975, 1977, 1978].

APPENDIX B: EVALUATION OF THE WIND SEA MODEL

It can be argued that the complete finite-depth wave model is unnecessary for applications under tropical cyclones (H. Graber, personal communication, 1990), so subroutines pertaining to the exchange of energy between the spectral swell model and the parametric wind sea model have been removed in this study. Thus any energy which should be transferred to swell was permanently lost from the wave field. Before using this simplified model, a series of comparisons was conducted to evaluate the validity of the wind sea assumption for the region of strongest winds within a tropical cyclone. The abbreviated model was compared first with the full model, as discussed by Graber and Madsen [1988] (GM), and then with wave spectra from storm-dominated ocean environments. Table B1 presents the results for both f_m and $H_{1/3}$ under the conditions of a sloping bottom (10^{-4} gradient), a friction factor of $f_w = 0.03$, and a 20-m/s steady wind. The difference increases with decreasing depth and is unacceptable at the limiting depth of 10 m. However, a depth of 10 m falls at the landward edge of the model grid, where shoreface processes are expected to dominate.

The performance of the wind sea model was then evaluated by comparison to storm wave spectra for different depths and bottom conditions: (1) shallow water spectra for the fetch- and duration-limited Texel storm from the North Sea with a sand substrate [Bouws and Komen, 1983] and (2) deepwater and shallow water spectra for Hurricane Frederic in the mud-bottomed Mississippi River delta region [Forristall and Reece, 1985]. These storm conditions were not hindcast but, instead, were simulated using uniform, steady winds and reasonable fetches in order to identify major problems with the wind sea model. For the Texel storm, a constant depth of 35 m was used, the wind was 25 m/s, and f_w was 0.03. The modeled and measured spectra for the Texel storm are similar, with the observed spectrum being slightly less peaked (Figure B1a) and giving no indication of swell. The observed values of f_m and $H_{1/3}$ were 0.086 s⁻¹ and 6.8 m, respectively. Those from the model were 0.0879 s⁻¹ and 6.02 m, giving differences of -2.21% and -11%, respectively. The spectra measured at the

TABLE B1. Comparison of Wind Sea Model Results to GM

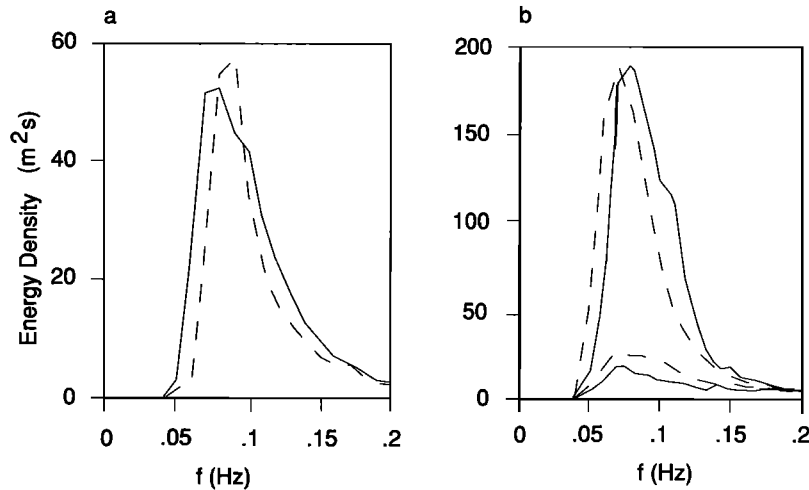| Depth m	f_m s⁻¹			$H_{1/3}$ m		
	GM	Model	Difference %	GM	Model	Difference %
10	0.0820	0.0475	-42	2.29	2.07	-9.61
20	0.0772	0.0690	-11	3.77	3.44	-8.7
30	0.0745	0.0748	+0.403	5.26	4.88	-7.22
60	0.0725	0.0744	+2.62	8.41	8.16	-2.97
120	0.0667	0.0708	+6.15	9.62	8.89	-7.59

Fig. B1. Spectra for the wind sea model (dashed line) compared against measured data for (a) the Texel storm (solid line) [Bouws and Komen, 1983] and (b) the spectra measured at Cognac platform (solid large line) and the inshore station (solid smaller line) during Hurricane Frederic [Forristall and Reece, 1985].

Cognac oil platform and the shallow water station by *Forristall and Reece* [1985] show the effects of bottom dissipation in a region of muddy substrate. Using a steep slope (0.007), a steady wind of 29 m/s, and $f_w = 0.1$ to simulate strong wave attenuation, the wind sea model produced spectra not too different from those observed (Figure B1b). In fact, for the Cognac platform the calculated f_m was smaller than the observed (0.0779 versus 0.08 s^{-1}), with the modeled $H_{1/3}$ greater (10.1 against 8.59 m). The Cognac spectrum does not contain a strong low-frequency component. Because of the deformable mud bottom reported at the shallow site, the model failed to sufficiently dissipate the wave energy, and $H_{1/3}$ was significantly overestimated (5.19 versus 2.45 m, a difference of +112%).

REFERENCES

Atkinson, C. D., M. J. Goeston, A. Speksnijder, and W. van der Vlugt, Storm-generated sandstone in the Miocene Miri formation, Seria field, Brunei (northwest Bornea), in Shelf Sands and Sandstones Reservoirs, edited by R. J. Knight and J. R. McLean, *Mem. Can. Soc. Pet. Geol., 11,* 213-240, 1986.

Bouma, A. H., H. L. Berryhill, H. J. Knebel, and R. I. Brenner, Continental shelf, in *Sandstone Depositional Environments,* edited by P. A. Scholle and S. Darwin, 410 pp., American Association of Petroleum Geologists., Tulsa, Okla., 1982.

Bouws, E., and G. J. Komen, On the balance between growth and dissipation in an extreme depth-limited wind-sea in the southern North Sea, *J. Phys. Oceanogr., 13,* 1653-1658, 1983.

Brenchley, P. J., Storm influenced sandstone beds, *Mar. Geol., 9,* 369-396, 1985.

Brenchley, P. J., M. Romano, and J. C. Guttierrez-Marco, Proximal and distal hummocky cross-stratified facies on a wide Ordovician shelf in Iberia, in Shelf Sands and Sandstones Reservoirs, edited by R. J. Knight and J. R. McLean, *Mem. Can. Soc. Pet. Geol., 11,* 241-256, 1986.

Cooper, C., and J. D. Thompson, Hurricane-generated currents on the outer continental shelf, 1., Model formulation and verification, *J. Geophys. Res., 94,* 12,513-12,539, 1989.

Craft, J. H., and J. S. Bridge, Shallow-marine sedimentary processes in the Late Devonian Catskill Sea, New York State, *Geol. Soc. Am. Bull., 98,* 338-355, 1987.

Curray, J. R., Sediments and history of Holocene transgression, continental shelf, northwest Gulf of Mexico, in *Recent Sediments, Northwest Gulf of Mexico,* edited by F. P. Shepard and T. H. van Andel, pp. 221-266, American Association of Petroleum Geologists, Tulsa, Okla., 1960.

Denness, B. (Ed.), *Seabed Mechanics,* 281 pp., Graham and Trotman, London, 1984.

Dott, R. H., and J. Bourgeois, Hummocky stratification: Significance of its variable bedding sequences, *Geol. Soc. Am. Bull., 93,* 663-680, 1982.

Duke, W. L., Hummocky cross-stratification, tropical hurricanes, and intense winter storms, *Sedimentology, 32,* 167-194, 1985.

Duke, W. L., Geostrophic circulation or shallow marine turbidity currents? The dilemma of paleoflow patterns in storm-influenced prograding shoreline systems, *J. Sediment. Petrol., 60,* 870-883, 1990.

Duke, W. L., R. W. C. Arnott, and R. J. Cheel, Shelf sandstones and hummocky cross-stratification: New insights on a stormy debate, *Geology, 19,* 625-628, 1991.

Einsele, G., and A. Seilacher (Eds.), *Cyclic and Event Stratification,* 536 pp., Springer-Verlag, New York, 1982.

Forristall, G. Z., and A. M. Reece, Measurements of wave attenuation due to a soft bottom: The SWAMP experiment, *J. Geophys. Res., 90,* 3367-3380, 1985.

Forristall, G. Z., R. C. Hamilton, and V. J. Cardone, Continental shelf currents in Tropical Storm Delia: Observations and theory, *J. Phys. Oceanogr., 7,* 532-546, 1977.

Forristall, G. Z., E. G. Ward, V. J. Cardone, and L. E. Borgmann, The directional spectra and kinematics of surface gravity waves in Tropical Storm Delia, *J. Phys. Oceanogr., 8,* 888-909, 1978.

Gagan, M. K., A. R. Chivas, and A. L. Herczeg, Shelf-wide erosion, deposition, and suspended sediment transport during Cyclone Winifred, central Great Barrier Reef, Australia, *J. Sediment. Petrol., 60,* 456-470, 1990.

Glenn, S. M., and W. D. Grant, A suspended sediment stratification correction for combined wave and current flows, *J. Geophys. Res., 92,* 8244-8264, 1987.

Goldring, R., and P. Bridges, Sublittoral sheet sandstones, *J. Sediment. Petrol., 43,* 736-747, 1973.

Graber, H. C., and O. S. Madsen, A finite-depth wind-wave model, I, Model description, *J. Phys. Oceanogr., 18,* 1465-1483, 1988.

Graber, H. C., R. C. Beardsley, and W. D. Grant, Storm-generated surface waves and sediment resuspension in the East China and Yellow seas, *J. Phys. Oceanogr., 19,* 1039-1059, 1989.

Grant, W. D., and S. M. Glenn, Continental shelf bottom boundary layer model, vol. I, Theoretical model development, final report to Pipeline Res. Comm. Project PR-153-126, Arlington, Va., Am. Gas Assoc., 1983.

Harms, J. C., J. B. Southard, and R. G. Walker, *Structures and Sequences in Clastic Rocks, Short Course 9,* Society of Economic Paleontologists and Mineralogists, Tulsa, Okla., 1982.

Harris, D. L., Meteorological aspects of storm surge generation, *J.*

Hydraul. Div. Am. Soc. Civ. Eng., 84, 231-243, 1958.

Hayes, M. O., Hurricanes as geological agents: Case studies of Hurricanes Carla, 1961, and Cindy, 1963, *Rep. of Invest. 61*, 54 pp., Tex. Bur. of Econ. Geol., Austin, Texas, 1967.

Ichiye, T., Circulation changes caused by hurricanes, in *Contributions on the Physical Oceanography of the Gulf of Mexico*, edited by L. R. A. Capurro and J. L. Reid, pp. 229-257, Gulf, Houston, Texas, 1972.

Jelesnianski, C. P., Numerical computations of storm surges without bottom stress, *Mon. Weather Rev., 94*(6), 379-394, 1966.

Kachel, N. B., and J. D. Smith, Geological impact of sediment transporting events on the Washington continental shelf, in *Shelf Sands and Sandstone Reservoirs*, edited by R. J. Knight and J. R. McLean, *Mem. Can. Soc. Pet. Geol., 11*, 145-162, 1986.

Keen, T. R., A three-dimensional numerical investigation of storm event bed genesis on the Texas-Louisiana continental shelf, Ph.D. thesis, 371 pp., Pa. State Univ., University Park, 1992.

Keen, T. R., and R. L. Slingerland, Four storm event beds and the tropical cyclones that produced them: A numerical hindcast, *J. Sediment. Petrol., 63, No. 2*, in press, 1993.

Kumar, N., and J. E. Sanders, Characteristics of shoreface storm deposits: Modern and ancient examples, *J. Sediment. Petrol., 46*, 145-162, 1976.

Leendertse, J. J., and S. K. Liu, A three-dimensional model for estuaries and coastal seas, vol. II, Aspects of computation, *Rep. R-1764-OWRT*, 123 pp., Rand Corp., Santa Monica, Calif., 1975.

Leendertse, J. J., and S. K. Liu, A three-dimensional model for estuaries and coastal seas, vol. IV, Turbulent energy computation, *Rep. R-2187-OWRT*, 59 pp., Rand Corp., Santa Monica, Calif., 1977.

Leendertse, J. J., and S. K. Liu, A three-dimensional turbulent energy model for nonhomogeneous estuaries and coastal sea systems, in *Hydrodynamics of Estuaries and Fjords*, edited by J. C. J. Nihoul, pp. 387-405, Elsevier Science, New York, 1978.

Leendertse, J. J., R. C. Alexander, and S. K. Liu, A three-dimensional model for estuaries and coastal seas, vol. I, Principles of computation, *Rep. R-1417-OWRR*, 57 pp., Rand Corp., Santa Monica, Calif., 1973.

Liu, S. K., and J. J. Leendertse, Three-dimensional subgridscale energy model of eastern Bering Sea, in *Proceedings, Coastal Engineering*, pp. 1-21, American Society of Civil Engineers, New York, 1978.

Liu, S. K., and J. J. Leendertse, A three-dimensional model for estuaries and coastal seas, vol. VI, Bristol Bay simulations, *Rep. R-2405-NOAA*, 121 pp.,Rand Corp., Santa Monica, Calif., 1979.

Lyne, V. D., B. Butman, and W. D. Grant, Sediment movement along the U. S. east coast continental shelf, I., Estimates of bottom stress using the Grant-Madsen model and near-bottom wave and current measurements, *Cont. Shelf Res., 10*, 397-428, 1990.

Martin, P. J., Mixed-layer simulation of buoy observations taken during Hurricane Eloise, *J. Geophys. Res., 87*, 409-427, 1982.

Morton, R. A., Formation of storm deposits by wind-forced currents in the Gulf of Mexico and the North Sea, in *Holocene Marine Sedimentation in the North Sea Basin, Spec. Publ.*, vol. 5, edited by S. D. Nio, R. T. E. Shuttenhelm, and T. C. E. van Weering, pp. 385-396, International Association of Sedimentologists, New York, 1981.

Morton, R. A., Nearshore responses to great storms, *Spec. Pap. 229*, 7-22, Geol. Soc. of Am., 1988.

Niedoroda, A. W., D. J. P. Swift, T. S. Hopkins, and C. M. Ma, Shoreface morphodynamics on wave-dominated coasts, *Mar. Geol., 60*, 331-354, 1984.

Niiler, P. P., Mixed-layer physics, in *Topics in Ocean Physics*, edited by A. R. Osborne and P. M. Rizzoli, pp. 339-370, North-Holland, New York, 1982.

Nittrouer, C. A., J. M. Coleman, R. D. Flood, R. N. Ginsburg, D. S. Gorsline, A. C. Hine, R. W Sternberg, D. J. P. Swift, and L. D. Wright, Sedimentation of continental margins: An integrated program for innovative studies during the 1990's, *Eos Trans. AGU, 69*, 58-69, 1988.

Nummedal, D., and J. W. Snedden, Sediment exchange between the shoreface and continental shelf--evidence from the modern Texas coast and the rock record, in *Coastal Sediments '87*, pp. 2110-2125, Houston, Texas 1987.

Pond, S., and G. L. Pickard, *Introductory Dynamical Oceanography*, 329 pp., Pergamon, New York, 1983.

Rahuel, J. L., F. M. Holly, P. J. Belleudy, and G. Yang, Modeling of riverbed evolution for bedload sediment mixtures, *J. Hydraul. Eng., 115*, 1521-1542, 1989.

Sanford, T. B., P. G. Black, J. R. Haustein, J. W. Feeney, G. Z. Forristall, and J. F. Price, Ocean response to a hurricane, I:, Observations, *J. Phys. Oceanogr., 17*, 2065-2083, 1987.

Sheng, Y. P., Mathematical modeling of three-dimensional currents and sediment dispersion: Model development and application, *Tech. Rep. CERC-83-2*, 288 pp., Coastal Eng. Res. Cent., Vicksburg, Miss., 1983.

Snedden, J. W., and D. Nummedal, Coherence of surf zone and shelf current flow on the Texas (USA) coastal margin: Implications for interpretation of paleo-current measurements in ancient coastal sequences, *Sediment. Geol., 67*, 221-236, 1990.

Snedden, J. W., D. Nummedal, and A. F. Amos, Storm- and fair-weather combined flow on the central Texas continental shelf, *J. Sediment. Petrol., 58*, 580-595, 1988.

Swift, D. J. P., and A. W. Niedoroda, Fluid and sediment dynamics on continental shelves, in *Shelf Sands and Sandstones, Short Course 13*, edited by R. W. Tillman, D. J. P. Swift, and R. G. Walker, pp. 47-133, Society of Economic Paleontologists and Mineralogists, Tulsa, Okla., 1985.

Swift, D. J. P., J. P. Han, and C. E. Vincent, Fluid processes and sea floor response on a modern storm-dominated shelf: Middle Atlantic shelf of North America, 1, The storm current regime, in *Shelf Sands and Sandstone Reservoirs*, edited by R. J. Knight and J. R. McLean, *Mem. Can. Soc. Pet. Geol., 11*, 99-109, 1986.

Swift, D. J. P., P. M. Hudelson, R. L. Brenner, and P. Thompson, Shelf construction in a foreland basin: Storm beds, shelf sand bodies, and shelf-slope sequences in the Upper Cretaceous Mesaverde Group, Book Cliffs, Utah, *Sedimentology, 34*, 423-457, 1987.

van Niekerk, A., K. R. Vogel, R. L. Slingerland, and J. S. Bridge, Routing of heterogeneous size-density sediments over a movable stream bed: Model development, *J. Hydraul. Eng., 118*, 246-262, 1992.

Vincent, C. E., Processes affecting sand transport on a storm-dominated shelf, in *Shelf Sands and Sandstone Reservoirs*, edited by R. J. Knight and J. R. McLean, *Mem. Can. Soc. Pet. Geol., 11*, 121-132, 1986.

Vogel, K. R., A. van Niekerk, R. L. Slingerland, and J. S. Bridge, Routing of heterogeneous size-density sediments over a movable stream bed: Model verification and testing, *J. Hydraul. Eng., 118*, 263-279, 1992.

Walker, R. G., Shelf and shallow marine sands, in *Facies Models, Geol. Assoc. Can. Reprint Ser.*, vol. 1, edited by R. G. Walker, pp. 141-170, Ainsworth, Kitchener, Ontario, Canada, 1984.

Zilitinkevich, S. S., D. L. Lajchtman, and A. S. Monin, Dynamics of the atmospheric boundary layer, *Atmos. Ocean Phys., 3*, 1231-1239, 1967.

T. R. Keen, Institute of Marine and Coastal Sciences, Rutgers University, P.O. Box 231, New Brunswick, NJ 08903.

R. L. Slingerland, Department of Geosciences, Pennsylvania State University, University Park, PA 16802.